Historical and future changes in global flood magnitude – evidence from a model-observation investigation

Hong Xuan Do[(1)(2)(3)(*)], Fang Zhao[(4)(5)(*)], Seth Westra[(1)], Michael Leonard[(1)], Lukas Gudmundsson[(6)], Julien Eric Stanislas Boulange[(7)], Jinfeng Chang[(8)], Philippe Ciais[(8)], Dieter Gerten[(5)(9)], Simon N. Gosling[(10)], Hannes Müller Schmied[(11)(12)], Tobias Stacke[(13)], Camelia-Eliza Telteu[(11)], Yoshihide Wada[(14)].

(1) School of Civil, Environmental and Mining Engineering, University of Adelaide, Adelaide, Australia.
(2) Faculty of Environment and Natural Resources, Nong Lam University, Ho Chi Minh City, Vietnam.
(3) School for Environment and Sustainability, University of Michigan, Ann Arbor, Michigan, United States.
(4) School of Geographical Sciences, East China Normal University, Shanghai, China.
(5) Potsdam Institute for Climate Impact Research, Potsdam, Germany.
(6) Institute for Atmospheric and Climate Science, Department of Environmental Systems Science, ETH Zurich, Zurich, Switzerland.
(7) Center for Global Environmental Research, Japan.
(8) Laboratoire des Sciences du Climat et de l'Environnement, CEA-CNRS-UVSQ/IPSL, Université Paris Saclay, 91191 Gif sur Yvette, France.
(9) Geography Dept., Humboldt-Universität zu Berlin, Berlin, Germany.
(10) School of Geography, University of Nottingham, Nottingham, United Kingdom.
(11) Institute of Physical Geography, Goethe University Frankfurt, Frankfurt am Main, Germany.
(12) Senckenberg Leibniz Biodiversity and Climate Research Centre (SBiK-F), Frankfurt am Main, Germany.
(13) Institute of Coastal Research, Helmholtz-Zentrum Geesthacht (HZG), Geesthacht, Germany.
(14) International Institute for Applied Systems Analysis, Laxenburg, Austria.

[(*)] *Corresponding authors:* Hong Xuan Do (hong.do@adelaide.edu.au) *and* Fang Zhao (fangzhao@pik-potsdam.de)

Abstract. To improve the understanding of trends in extreme flows related to flood events at the global scale, historical and future changes of annual maximum of 7-day streamflow are investigated, using a comprehensive streamflow archive and six global hydrological models. The models' capacity to characterise trends in annual maximum of 7-day streamflow at the continental and global scale is evaluated across 3,666 river gauge locations over the period from 1971 to 2005, focusing on four aspects of trends: (i) mean, (ii) standard deviation, (iii) percentage of locations showing significant trends and (iv) spatial pattern. Compared to observed trends, simulated trends driven by observed climate forcing generally have a higher mean, lower spread, and a similar percentage of locations showing significant trends. Models show a low-to-moderate capacity to simulate spatial patterns of historical trends, with approximately only 12-25% of the spatial variance of observed trends across all gauge stations accounted for by the simulations. Interestingly, there are statistically significant differences between trends simulated by GHMs forced with observational climate and forced by bias corrected climate model output during the historical period, suggesting the important role of the stochastic natural (decadal, inter-annual) climate variability. Significant differences were found in simulated flood trends when averaged only at gauged locations compared to when averaged across all simulated grid cells, highlighting the potential for bias toward well-observed regions in the state-of-understanding of changes in floods. Future climate projections (simulated under RCP2.6 and RCP6.0 greenhouse gas concentration scenario) suggest a potentially high level of change in individual regions, with up to 35% of cells showing a statistically significant trend (increase or decrease; at 10% significance level) and greater changes indicated for the higher concentration pathway. Importantly, the observed streamflow database under-samples the percentage of locations consistently projected with increased flood hazards under RCP6.0 greenhouse gas concentration scenario by more than an

order of magnitude (0.9% compared to 11.7%). This finding indicates a highly uncertain future for both flood-prone communities and decision makers in the context of climate change.

1 Introduction

Global hydrological models (GHMs) are critical tools for diagnosing factors of rising trends in flood risk (Munich Re, 2015;Swiss Re, 2015;Miao, 2018;Smith, 2003;Guha-Sapir et al., 2015;CRED, 2015), and can help identify the contribution of changing flood hazard characteristics relative to the changing exposure of human assets to floods. GHMs are also used to project future changes in flood hazard, owing to their ability to simulate streamflow under projected atmospheric forcing. Using GHM simulations, several studies have found more regions showing increasing trends than decreasing trends in flood hazards at the global scale, and have attributed these changes to anthropogenic climate change (Dankers et al., 2014;Arnell and Gosling, 2014;Alfieri et al., 2015;Kettner et al., 2018;Willner et al., 2018;Asadieh and Krakauer, 2017). The pattern of increasing trends obtained from GHM simulations is consistent with observations of increases in precipitation extremes (Westra et al., 2013;Westra et al., 2014;Donat et al., 2013;Guerreiro et al., 2018) that have been used by a number of studies as a proxy to suggest that flood hazard may increase as a result of climate change (Alfieri et al., 2017;Pall et al., 2011;IPCC, 2012;Forzieri et al., 2016).

The inference of changes in flood hazard following the same direction as extreme precipitation may be appropriate over regions where rainfall plays the dominant role in flood occurrence (Hoegh-Guldberg et al., 2018;Mallakpour and Villarini, 2015;Mangini et al., 2018), but recent evidence based on instrumental trends in flood hazard suggests it is not necessarily globally applicable (Ivancic and Shaw, 2015;Blöschl et al., 2019). This is due to a 'dichotomous relationship' between trends exhibited in extreme precipitation and extreme streamflow (Sharma et al., 2018), highlighted in recent observation-based studies of trends in streamflow magnitudes (Wasko and Sharma, 2017;Do et al., 2017;Hodgkins et al., 2017;Gudmundsson et al., 2019). The hypothesised reason for this potentially inconsistent relationship is the complexity of the drivers of flood risk (Johnson et al., 2016;Blöschl et al., 2017;Do et al., 2019;Berghuijs et al., 2016), with the implication that historical and future changes to flood hazard at the global scale are unlikely to be reflected by changes to a single proxy variable alone, such as annual maximum rainfall. For example, even though trends in extreme flows are highly correlated to changes in extreme rainfall when rainfall plays the dominant role (Mallakpour and Villarini, 2015;Blöschl et al., 2017), snowmelt-related flood magnitude has been found to decrease in a warmer climate, potentially due to a shift in snowmelt timing (Burn and Whitfield, 2016;Cunderlik and Ouarda, 2009). The sign of change is also unclear for locations where antecedence soil moisture plays an important role (Woldemeskel and Sharma, 2016;Sharma et al., 2018), owing to the combined influences of seasonal/annual precipitation, potential evaporation and extreme

precipitation (Bennett et al., 2018;Ivancic and Shaw, 2015;Leonard et al., 2008;Wasko and Nathan, 2019). The sensitivity of changes in streamflow to anthropogenic influences such as urbanization, dams and reservoir operations, or river morphology (FitzHugh and Vogel, 2011;Slater et al., 2015) further suggests that it is not possible to use trends in extreme precipitation alone to infer changes in flood hazards.

To better understand historical and future trends in streamflow, the emphasis has therefore moved to analysing trends directly in streamflow measurements. Investigations using streamflow observations at global, continental and regional scales (see Do et al. (2017) and references therein) have generally detected a mixed pattern of trends, with some global-scale studies finding more stations having decreasing trends than increasing trends (Do et al., 2017;Hodgkins et al., 2017;Kundzewicz et al., 2004). These conclusions appear *prima facie* to be inconsistent with model-based evidence, which generally suggests the opposite (more locations showing increasing trends). However, varying sampling strategies, statistical techniques and reference periods make it difficult to derive a common perspective of trends in global flood hazards from a composite of observational and modelling studies. In addition, data coverage limitations (Hannah et al., 2011;Gupta et al., 2014;Do et al., 2018a) remain a barrier to reliably benchmarking trends over some areas such as the flood-prone regions of South and East Asia.

GHMs, with the advantage of better spatial coverage, remain an important line of evidence about historical and future trends. GHMs also enable the possibility to explore the individual roles of atmospheric forcing, land use change and other drivers of change on streamflow trends by including or excluding a specific factor from simulation setting. However, no study has evaluated the performance of GHMs in terms of reproducing trends of streamflow indices, including flood indicators. To date, GHMs have been assessed extensively on their capacity to represent physical features of the hydrological regime, such as streamflow percentiles, the seasonal cycle, or the timing of peak discharge (Gudmundsson et al., 2012a;Zaherpour et al., 2018;Beck et al., 2017;Zhao et al., 2017;Veldkamp et al., 2018;Pokhrel et al., 2012;Biemans et al., 2011;Giuntoli et al., 2018). Nevertheless, streamflow variability can be subject not only to long-term changes in atmospheric forcing, but also to climate variability (e.g. inter-annual, inter-decadal) as well as human activities across the drainage basin (Zhang et al., 2015;Zhan et al., 2012). Thus, the GHMs' capacity to represent physical features of a hydrological regime is not necessarily sufficient to determine their performance in simulating characteristics of trends. The absence of a holistic understanding of GHMs' capacity to simulate trends implies that model-based inferences on changes in flood hazards are highly uncertain (Dankers et al., 2014), limiting the usefulness of GHMs in developing flood adaptation policy in a warming climate.

To address this limitation and further improve GHMs' applicability, this study provides the first comprehensive evaluation of GHMs' capacity in simulating historical trends of a flood hazard indicator. This study also explores the uncertainty in developing projected changes in flood hazards using GCMs-GHMs ensemble. Specifically, we used the Global Streamflow Indices and Metadata (GSIM) archive (Do et al., 2018b;Gudmundsson et al., 2018), to-date the largest possible global streamflow database, to identify observed changes in annual maximum of 7-day streamflow (MAX7 index) over the 1971-2005 period. Streamflow simulations, available through the Inter-Sectoral Impact Model Intercomparison Project ISIMIP phase 2a and 2b (Warszawski et al., 2014), were used to derive historical (1971-2005) and projected (2006-2099) changes in MAX7 index simulated by GHMs. Observed and simulated trends were then analysed to achieve three research objectives.

- Objective 1: to evaluate the capacity of GHMs to reproduce observed trends of an indicator of flood hazard (MAX7). The particular interest is in reconciling model- and observation-based inferences of historical changes in flood hazard at the global and continental scale.
- Objective 2: to determine the representativeness of observation locations (streamflow gauges) in GHM simulations. This objective is motivated by the sparse coverage of streamflow observations over several regions (e.g. South and East Asia), which could lead to biased inferences of observation-based studies over large spatial domains wherever gauges are not a representative sample.
- Objective 3: to assess the implication of model uncertainty for projections of flood hazard, focusing on the uncertainty of the mean/spread of trends together with the spatial pattern of trends in annual maximum streamflow. We are also curious of whether the regions consistently projected with an increase in flood have been adequately observed by the global observation networks.

2 Data and methods

This section summarizes the workflow to achieve three objectives of this study (Figure 1). Observed and simulated streamflow (section 2.1) were used to estimate the magnitude and significance of changes in an indicator of flood hazards (section 2.3). To enable an observation-model comparison, a procedure was developed to extract streamflow for a subset of observed catchments that meet data quality criteria (section 2.2). A range of statistical techniques were then applied to trends of an indicator of flood magnitude (section 2.4) to assess (i) the capacity of GHMs to reproduce characteristics of observed trends, (ii) the representativeness of observation locations in GHM simulations, and (iii) the implication of simulation uncertainty on projected trends (results are discussed in sections 3.1, 3.2, and 3.3).

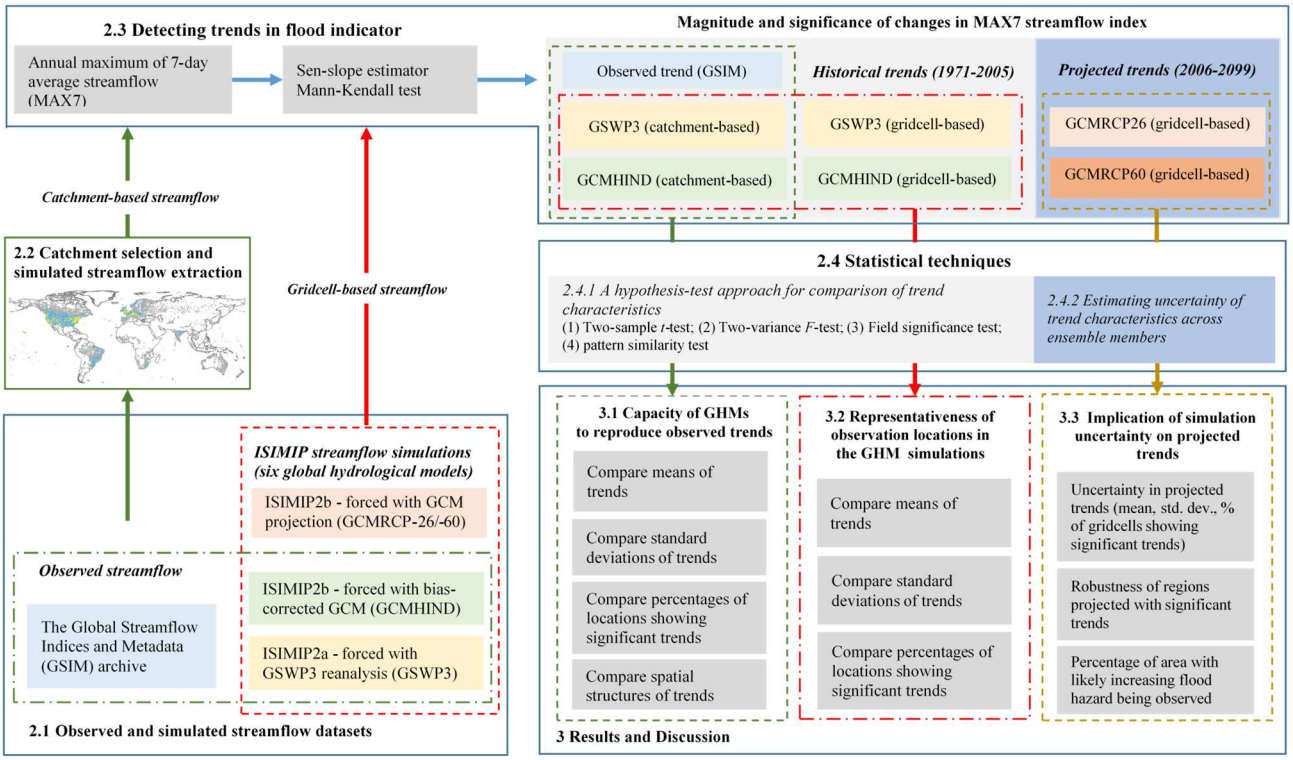

Figure 1. Flowchart of the datasets and methodologies used to achieve three research objectives of this study.

2.1 Observed and simulated streamflow datasets

The GSIM archive is used as daily observational discharge for this analysis. Daily streamflow simulations available through the ISIMIP are used, with historical simulations (forced with observational climate in ISIMIP2a and bias-corrected climate model outputs in ISIMIP2b) spanning from 1971 to 2005 (Gosling et al., 2019) and future simulations (ISIMIP2b) covering 2006-2099 period (Frieler et al., 2017). Six GHMs are considered: H08 (Hanasaki et al., 2008b, a), LPJmL (Schaphoff et al., 2013), MPI-HM (Stacke and Hagemann, 2012), ORCHIDEE (Guimberteau et al., 2014;Guimberteau et al., 2018), PCR-GLOBWB (Wada et al., 2014;Sutanudjaja et al., 2018), and WaterGAP2 (Müller Schmied et al., 2014;Mueller Schmied et al., 2016). These models were selected as they have provided discharge data within phases 2a and 2b of ISIMIP at the time this study began (June 2018). A summary of the similarities and differences across participated GHMs is provided in supplementary section 1.2.

To assess the model structural uncertainty across GHMs, trends in streamflow extremes simulated under observational atmospheric forcing, available through the Global Soil Wetness Project Phase 3 (GSWP3) reanalysis (Kim, 2017), were compared to observed trends. The influence of the high uncertainty in climate models (Kumar et al., 2013;Kiktev et al., 2003) on streamflow simulations was assessed by comparing observed trends and trends simulated when using

atmospheric forcing from four General Circulation Models (GCMs) for the historical period ('hindcast' simulations; hereafter referred to GCMHIND atmospheric forcing). These GCMs were bias corrected but their simulations have different sub-monthly, inter-annual and decadal variability and thus the hindcast simulations reflect both GHM and GCM uncertainty. To quantify the implication of model uncertainty for future projections of flood hazard, trends simulated under projected climate change by the end of this century (using the same four GCMs) were also assessed for two greenhouse gas concentration scenario RCP2.6 (hereafter referred to GCMRCP2.6 atmospheric forcing) and RCP6.0 (hereafter referred to GCMRCP6.0 atmospheric forcing). As a result, four simulation settings were used in this study, denoted by the atmospheric forcing; an overview is given in Table 1. These settings comprise two historical runs (GSWP3 and GCMHIND runs), and two future runs (GCMRCP2.6 and GCMRCP6.0), collectively amounting to a total of 69 simulations (see Table S3 in supplementary with full list of simulations).

For GSWP3 simulations, a preliminary analysis (see section 4 of supplementary material) shows that both 'naturalised runs' (i.e. human water management not taken into account) and 'human impact runs' (i.e. human water management inputs were used) exhibit similar characteristic of trends in MAX7 index. Some potential reasons for negligible impacts of human water management are the spatial distribution of stream gauges (may be biased toward regions with insignificant changes in water management during the 1971-2005 period), or the inclusion of small catchments (more that 3,000 catchments with reported area less than 9,000 km^2), thus floods are more sensitive to changes in climate forcing relative to the accumulated basin-wide influence of human impacts. Naturalised runs were therefore chosen, since this setting is available for more GHMs (six) when compared to the human impact setting (four). Although significant efforts were made by ISIMIP to keep the setting across simulations as consistent as possible, there were some differences in model versions and input data (e.g., WaterGAP2.2 (ISIMIP2a) was used in ISIMIP2a while WaterGAP2.2c was used in ISIMIP2b; ORCHIDEE (Guimberteau et al., 2014) was used in ISIMIP2a while ORCHIDEE-MICT (Guimberteau et al., 2018), with improvements on high latitude processes, was used in ISIMIP2b). Although the influence of versioning is minor for WaterGAP2, the potential effects of technical discrepancies cannot be checked in the context of this study, as not all required simulations are readily available (see our discussion in supplementary section 3.3). In addition, owing to technical requirements across GHMs, different models do not have the same set of coastal cells, which may lead to some minor effect to the statistics when averaged across all simulation grid-cells.

Table 1. Summary of streamflow observation and simulation datasets used in this study. GSIM was used as the observed streamflow database. Streamflow simulations were obtained from six GHMs (H08, LJPmL, MPI-HM, ORCHIDEE, PCR-GLOBWB and WaterGAP2). One observational atmospheric forcing dataset (GSWP3) and outputs of four GCMs were used as input for streamflow simulations.

Reference window	Streamflow obs./sim.	No. of GCM-GHM combination	Description	Note
Historical (1971-2005)	GSIM	-	Observational streamflow selected from GSIM archive.	Streamflow daily observations for 3,666 unique locations
	GSWP3 (ISIMIP 2a)	6	Historical simulation forced by observational atmospheric forcing.	Model did not use human water management input.
	GCMHIND (ISIMIP 2b)	21	Historical simulation using atmospheric forcing from four GCMs: GFDL-ESM2M, HadGEM2-ES, IPSL-CM5A-LR and MIROC5.	No HadGEM2-ES simulation for MPI-HM.
Projection (2006-2099)	GCMRCP2.6 (ISIMIP 2b)	21	Future simulation forced by projected atmospheric forcing under greenhouse gas concentration scenario RCP2.6. Four GCMs were used: GFDL-ESM2M, HadGEM2-ES, IPSL-CM5A-LR and MIROC5.	No HadGEM2-ES and MIROC5 simulations for ORCHIDEE.
	GCMRCP6.0 (ISIMIP 2b)	21	Future simulation forced by projected atmospheric forcing under greenhouse gas concentration scenario RCP6.0. Four GCMs were used: GFDL-ESM2M, HadGEM2-ES, IPSL-CM5A-LR and MIROC5.	

2.2 Catchment selection and simulated streamflow extraction for observation-model comparison

To enable an observation-model comparison, simulated discharge needs to be extracted from gridded model output. Large-scale hydrological models, however, generally do not simulate discharge accurately over small-to-medium size catchments due to the coarse resolution of river network datasets in their routing schemes (Hunger and Döll, 2008). To address this limitation, previous GHMs evaluations usually selected large catchments (a threshold of 9,000 km^2 was adopted, approximating the size of a one-degree longitude/latitude grid cell) and routed discharge (units: m^3/s) at the outlet of the catchment was used as simulated streamflow for a specific catchment (Zhao et al., 2017;Veldkamp et al., 2018;Zaherpour et al., 2018;Liu et al., 2017;Zaherpour et al., 2019). For evaluation studies that used relatively small catchments (e.g. area less than 9,000 km^2), the un-routed runoff simulation (units: mm/day) was extracted while observed

183 discharge was converted to runoff using catchment area prior to comparison (Gudmundsson et al., 2012b;Beck et al.,
184 2017). To increase the sample size for the model-observation comparison (the first objective), the present study used both
185 daily (i) un-routed runoff for small catchments and (ii) routed discharge simulations for large ones, and thus two
186 extraction procedures were adopted. A summary of these extraction procedures is provided below while detailed technical
187 descriptions are provided in section 2 of supplementary material.

188 • For catchments with area from 0 to 9,000 km^2: un-routed runoff (mm/day) was extracted and then converted into
189 discharge (m^3/s) by multiplying averaged runoff with catchment area reported in station metadata. Specifically,
190 catchment boundaries were superimposed on the GHM grid to obtain the weighted-area tables, which were then
191 used to derive averaged runoff from the un-routed runoff simulation. To avoid double counting runoff from the
192 same grid points, runoff for catchments that share similar weighted-area tables (i.e. similar simulated streamflow
193 would be extracted – see supplementary section 2 for detail description) was averaged (using catchment areas as
194 weights) and a single 'averaged time series' was used in place of the runoff from the component catchments.
195 • For catchments with area greater than 9,000 km^2: the 'discharge output' approach (Zhao et al., 2017) was
196 adopted to extract routed discharge (m^3/s) from the GHM cell corresponding to the outlet of each catchment.

197 To ensure sufficient data is available for historical trend analysis, only GSIM stations with at least 30 years of data
198 available during the 1971-2005 period were considered (each year having at least 335 days of available records, implying
199 that annual maximum of a specific year is identified only when more than 90% of daily record is available). These
200 relatively strict selection criteria also enable a comparison between this study and preceding observation-based
201 investigations (Gudmundsson et al., 2019;Hodgkins et al., 2017). As catchment boundary shapefiles (Do et al., 2018a)
202 were used to extract simulated streamflow for small catchments, stations were further filtered using two criteria: (i)
203 availability of reported catchment area, and (ii) catchment boundary was accompanied with a "high" or "medium" quality
204 flag (i.e. the discrepancy between reported and estimated catchment area is less than 10%).

205 A total of 4,595 stations satisfied the quality selection criteria, of which large catchments (i.e. area greater than 9,000
206 km^2) where no suitable grid cell could be identified were further removed (11 catchments). For cases of two or more small
207 catchments (i.e. area less than or equal to 9,000km^2) having similar weighted-area tables, the 'averaged time series' (using
208 catchment areas as weights) was calculated. A total number of 1,542 time series fell in this category and were aggregated
209 into 624 'averaged time series'. Figure 2 shows the spatial distribution of the final dataset for model-observation
210 comparison, containing data for 3,666 locations (3,042 non-averaged time series and 624 averaged time series). The

majority of available catchments are located in North America and Europe, with some regions over Asia, Oceania and South America are also covered.

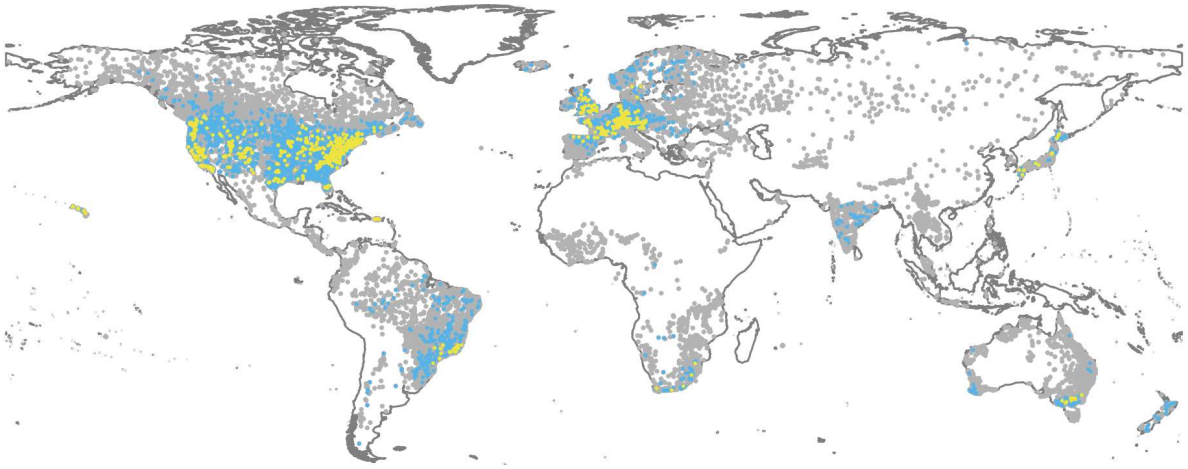

Figure 2. Locations of 3,666 streamflow observations (blue dots: 3,024 non-averaged time series; yellow dots: 624 averaged time series, where geographical coordinates were averaged from all component gauging coordinates) selected from GSIM archive for the model-observation comparison. Grey dots indicate GSIM time series that were removed due to insufficient data availability or quality.

2.3 Detecting trends in annual maximum streamflow

For each streamflow dataset, daily discharge was smoothed to 7-day averages to reduce variability in simulated streamflow, which can arise from the coarse routing parameters of GHMs (Dankers et al., 2014). The annual maximum time series of 7-day averaged discharge (labelled as the MAX7 index in the GSIM archive) was then derived to represent peak flow events. For gridded datasets, the 'centre averaged approach' (e.g. averaged streamflow of Jan 7th is the mean value of Jan 4 – 10th) was used (the common setting of the CDO software, freely available at https://code.mpimet.mpg.de/projects/cdo), and the MAX7 timeseries was therefore derived for each GSIM station using this same approach. As a result, the derived value of the MAX7 index is slightly different to the value available in the online version of GSIM , which applied a 'backward-moving average' technique (e.g. averaged streamflow of Jan 7th is the mean value of Jan 1 – 7th). Our preliminary analysis (not shown), however, indicated that this difference did not lead to substantial changes in the key findings (i.e., similar spatial composition between increasing and decreasing trends).

The magnitude of trends in the MAX7 index at a specific catchment or grid cell was quantified using the normalised Theil-Sen slope (Gudmundsson et al., 2019;Stahl et al., 2010) and the results are expressed in % change per decade. The significance of the local trend was assessed using a Mann-Kendall test at the 10% two-sided significance level (Wilks,

2011). The null hypothesis (no trend) is rejected if the two-sided *p*-value of the test statistic (Kendall's τ) is lower than 0.1, while the direction of the trend (i.e. increasing or decreasing) was determined using the sign of τ.

2.4 Statistical techniques

To explore GHMs' capacity to simulate observed trends and the implication of model uncertainty to projected trends, trends in streamflow extremes obtained from GSIM (observed trends) and ISIMIP simulations (simulated trends) are analysed. The observed trends were available for 3,666 observation locations. Simulated trends were available for all 59,033 GHM grid cells (estimated from routed discharge of each grid cell; Antarctica and Greenland were removed). To enable a model-observation comparison, we also extract a subset of simulated trends over the 3,666 observation locations (described in section 2.2).

2.4.1 A hypothesis-test approach for comparison of trend characteristics

A range of hypothesis tests (summarised in Table 2; GSWP3 simulations were used to assess GHM uncertainty while GCMHIND simulations were used to assess the combined GCM-GHM uncertainty) was applied to address the first two objectives, which require comparing trend characteristics exhibited from different streamflow datasets. Four characteristics of trends were assessed:

- Trend mean: The mean (% change per decade) of trends in streamflow extremes across all gauge-/cell-based time series over a spatial domain. A hypothesis test was adopted to assess whether the trend means exhibited from two specific streamflow datasets (e.g. model vs. observed) are significantly different from each other.
- Trend standard deviation: The standard deviation (% change per decade) of trends in streamflow extremes across all gauge-/cell-based time series over a spatial domain. A hypothesis test was adopted to assess whether the trend standard deviations exhibited from two specific streamflow datasets are significantly different from each other.
- Percentage of significant trends (%): The percentage of trends in a domain that are statistically significant, with gauge- or cell-based significance calculated using the Mann-Kendall test at the 10% significance level. To assess whether the percentage of significant (increasing/decreasing) trends exhibited from a specific streamflow dataset is produced by random chance, a field significance test (Do et al., 2017) was adopted (described in Table 2).
- Trend spatial pattern: The spatial distribution of trends in streamflow extremes over a spatial domain. Pearson's correlation (*r* statistic) (Galton, 1886;Kiktev et al., 2003) between trends of MAX7 index obtained from two datasets was used as a measure of similarity in the trend spatial structure. The hypothesis test (pattern similarity test) was adopted to assess whether: (i) the correlation between simulated trends introduced by GHMs and

observed trends is significantly higher than zero; and (ii) the correlation between trends simulated under hindcast atmospheric forcing and observed trends is significantly lower than that between trends simulated under observational atmospheric forcing and observed trends.

263 **Table 2.** Hypothesis tests conducted to address the first two objectives.

Objective	Null-Hypotheses	Streamflow dataset	Statistical tests
Objective 1: Capacity of GHMs to reproduce observed trends in flood hazards	Hypothesis 1: Trend means obtained from two streamflow datasets over observation locations were not statistically different from each other.	(i) Observed discharge across 3,666 observation locations (ii) Simulated discharge across 3,666 observation locations (extraction processes outlined in Section 2.2)	Two-sample *t*-test at the 10% two-sided significance level
	Hypothesis 2: Trend standard deviations obtained from two streamflow datasets over observation locations were not statistically different from each other.		Two-variance *F*-test at the 10% two-sided significance level
	Hypothesis 3: Percentage of significant trends obtained from all observation locations of a specific streamflow dataset was not produced by random chance.		Field significance test similar to that presented in Do et al. (2017) was adopted. A moving-block-bootstrap (block-length $L = 2$) was used to derive a null-hypothesis distribution of the change that occurred due to random chance. The null hypothesis is rejected at 5% one-sided significance level when the true percentage falls on the right-hand side of the 95th percentile of the resampled distributions.
	Hypothesis 4: The correlation between trends obtained from two streamflow datasets was not significantly higher than '0' (i.e. zero pattern similarity).		'Zero pattern similarity' was compared to the probability distribution function (PDF) of pairwise correlation between simulated and observed trends, drawn from a bootstrap procedure similar to that proposed by Kiktev et al. (2003). The null hypothesis is rejected at 5% one-sided significance level when zero correlation falls on the left-hand side of the 5th percentile of the resampled distributions.

	Hypothesis 5: The correlation between GCMHIND simulated trends and observed trends was not significantly lower than the correlation between GSWP3 simulated trends and observed trends		The actual pairwise correlation between GCMHIND simulated trends and observed trends (denoted by $r_{GCMHIND}$) was compared to the bootstrapped PDF of correlation exhibited from GSWP3 simulated trends (denoted by r^*_{GSWP3}). If $r_{GCMHIND}$ falls on the left-hand side of the 5th percentile r^*_{GSWP3}, there is evidence to reject the null-hypothesis at the 5% one-sided significance level.
Objective 2: The representativeness of observation locations in the GHM simulations	Hypothesis 6: Trend mean obtained from observation locations was not statistically different to that obtained from all grid cells.	(i) Simulated discharge across 3,666 observation locations (extraction processes outlined in Section 2.2)	Two-sample *t*-test at the 10% two-sided significance level
	Hypothesis 7: Trend standard deviation obtained from observation locations was not statistically different to that obtained from all grid cells.		Two-variance *F*-test at the 10% two-sided significance level
	Hypothesis 8: Percentage of significant trends obtained from all grid cells of a specific streamflow dataset was not produced by random chance.	(ii) Routed discharge across all landmass grid cells (59,033 cells)	Field significance test similar to that presented in Hypothesis 3 but trends obtained from all grid cells were the subject of the assessment.

264

2.4.2 Estimating uncertainty of trend characteristics across ensemble members

The third and final objective, which focused on the implications of GCM-GHM uncertainty on projected changes in flood hazard, was addressed by quantifying the spread of trend characteristics (i.e. trend mean, trend standard deviation, and percentage of significant trends) exhibited from routed discharge projections under two representative concentration pathways.

The spatial uncertainty of projected trends (GCMRCP2.6 and GCMRCP6.0) was also quantified by calculating intra-/inter-model correlation of the trend patterns across all ensemble members available under the two projections. Intra-model correlation represents spatial uncertainty introduced by the GCM and was calculated from simulated trends introduced by the same GHM (using different simulated atmospheric forcing). Inter-model correlation represents the combined GCM-GHM spatial uncertainty, and was calculated for each pair of simulated trends that were: (i) introduced by the different GHMs; and (ii) forced with different projected atmospheric forcing.

To assess the robustness of GHMs in projecting changes in flood hazard, each grid-cell available in the discharge simulation grid was then categorised into one of the five 'flood-risk' (here "flood-risk" level is defined as the number of ensemble members projecting significant increasing trends) groups based on the number of GCMRCP2.6/GCMRCP6.0 simulation members projecting a significant increasing trend (Group 1: no members, Group 2: from 1 to 5 members, Group 3: from 6 to 10 members, Group 4: from 11 to 15 members and Group 5: from 16 to 18 members).

Finally, to assess whether locations projected with an increasing trend by the majority simulations are adequately monitored, each GSIM gauge was allocated into one of these five groups based on the gauge's geographical coordinates. The allocation of gauges into these groups was then analysed to determine whether the most comprehensive global database of daily streamflow records to-date was evenly distributed across the five 'flood risk regions'. An inadequately coverage of stream-gauge networks over high risk regions indicate potentially high vulnerability to future changes in flood hazards, as insufficient data is available to inform decision makers.

3 Results and Discussion

3.1 Capacity of GHMs to reproduce observed trends in flood hazards

Visual inspection of the normalised Theil-Sen slope across the GSIM time series (top panel of Figure 3; regional maps provided in Supplementary Figure S4) shows a spatial pattern that is consistent with recent findings on trends in observed flood magnitude (Mangini et al., 2018;Do et al., 2017;Mallakpour and Villarini, 2015;Gudmundsson et al., 2019;Burn and Whitfield, 2018;Ishak et al., 2013). Specifically, decreasing trends tend to dominate Asia (most

294 stations located in Japan and India), Australia, the Mediterranean, western/north-eastern US and northern Brazil,
295 while increasing trends appear mostly over central North America, southern Brazil and the northern part of Western
296 Europe (including the UK). Note that the observation locations are not evenly distributed (86% in North America and
297 Europe), and thus the confidence of this assessment varies substantially across continents.

298 The multi-model average of GSWP3 simulated trends (trends simulated under observational atmospheric forcing;
299 middle panels of Figure 3) has generally good capacity to reproduce spatial patterns of observed trends. The multi-
300 model average of GCMHIND simulated trends (trends simulated under hindcast atmospheric forcing; lower panels of
301 Figure 3), however, could not reproduce some spatial agglomerations of trends in streamflow maxima (e.g. the
302 decreasing trends in south-eastern Australia, increasing trends over north-eastern Europe). This feature indicates the
303 inconsistent climate variability between GCMs and the real world, suggesting GCM climate forcing cannot account
304 for observed trends at sub-continental scale. In addition, GCMs uncertainty can potentially contribute to this
305 inconsitency. Interestingly, the multi-model average of both GSWP3 and GCMHIND simulations generally exhibits a
306 lower magnitude of changes (i.e. closer to 'zero change') compared to the observed trends. This feature is more
307 prominent in GCMHIND (21 simulations available) compared to GSWP3 (six simulations available), and can be
308 explained by two possibilities. The first possible explanation is the nature of averaging, which tends to smooth out
309 variability in trend magnitude across ensemble members, leading to a relatively 'close to zero' change across the
310 globe (given that each GCMs has stochastic decadal climate variability, so that averaging results forced by GCMs
311 tends to cancel trends). An alternative explanation is that individual simulations also exhibit a lower magnitude of
312 change relative to observation. As Figure 3 is not sufficient to evaluate the latter possibility, a more detailed
313 comparative analysis between observed trends and individual simulated trends using both historical climate forcings
314 (via GSWP3) and GCM hindcasts was conducted. Specifically, four characteristics of trends in extreme flows (i.e.
315 trend mean, trend standard deviation, percentage of significant trends and trend spatial structure) were assessed for
316 individual simulations and the results are reported in following sections. At the global scale, GSIM observed trends
317 exhibit a mean and standard deviation of -2.4% and 9.9% change per decade over the 1971-2005 historical period.
318 Furthermore, there are 7.5% (12.1%) stations showing significant increasing (decreasing) trends (detected by the
319 Mann-Kendall test at the 10% significance level). These numbers, however, are not statistically significant at the
320 global scale.

321

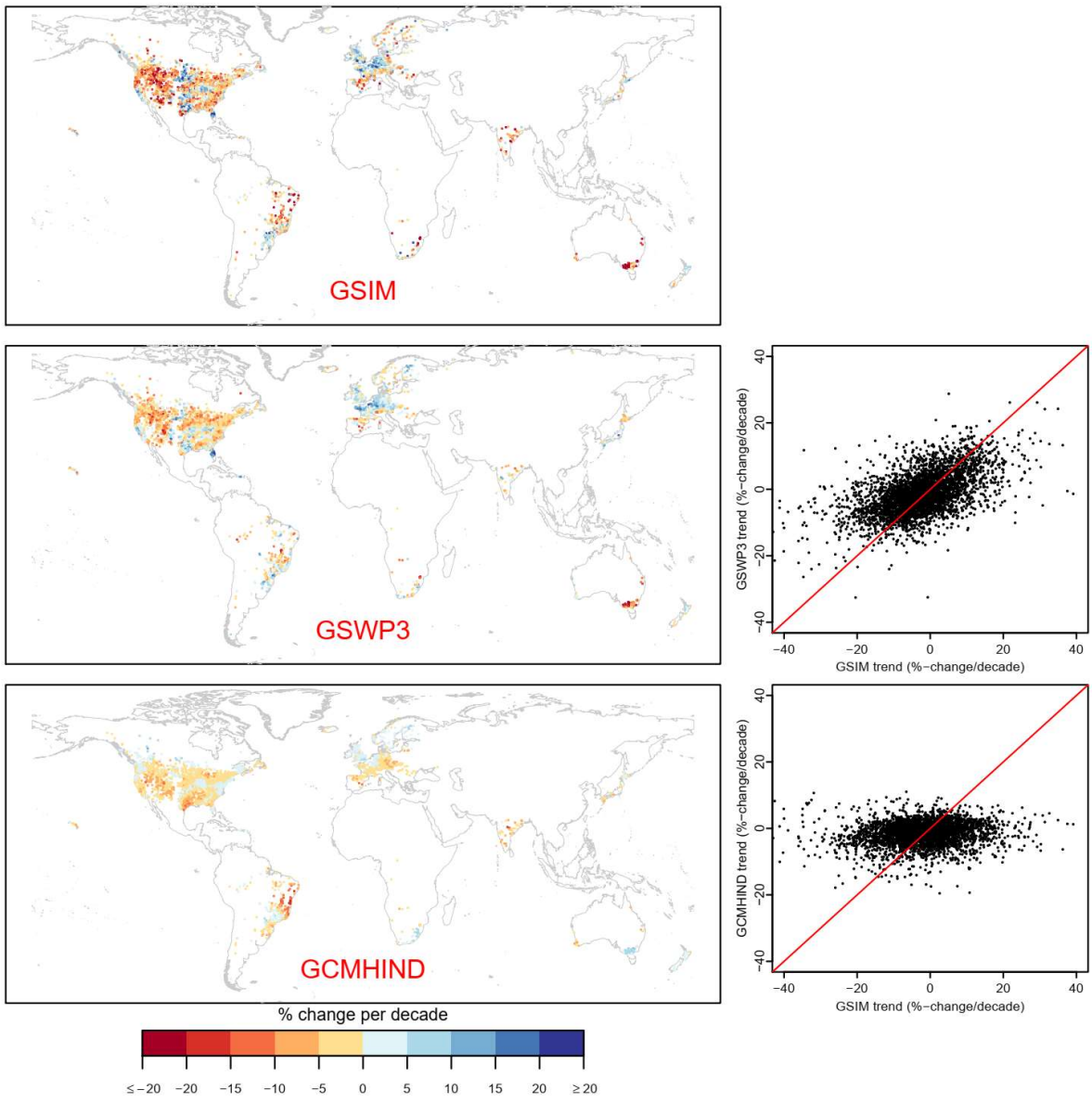

322

323 **Figure 3.** Normalised Theil-Sen slope for historical trends in flood magnitude (MAX7 index) exhibited over 3,666
324 locations across three streamflow datasets (top left: GSIM; middle left: GSWP3; bottom left: GCMHIND). Multi-
325 model average is shown for simulated trends. Trend is expressed in % change per decade. Scatter plot between trends
326 obtained from GSIM and GSWP3/GCMHIND simulated streamflow are provided in the right panels.

327

328 Table 3 shows the results of the global model-observation comparison using GSWP3 simulated trends across the six
329 GHMs. Compared to observed trends, most simulated trends have a significantly higher global trend mean at the
330 observed locations and lower trend standard deviation. The percentage of locations showing significant trends varies
331 substantially across simulations, but the values were not statistically significant. All GHMs demonstrate low-to-
332 moderate capacity in simulating the spatial pattern of trends (spatial correlation coefficients range from 0.35 to 0.50,

indicating that GSWP3 simulated trends account for between 12%-25% of the cross-location variability in the observed trend signal). There is, however, a notable difference in terms of the overall sign of trends simulated by each GHM. This feature indicates that using different GHMs can lead to different interpretations about the overall change in flood hazard at the global scale, despite having a common boundary forcing. Therefore, the 'closer to zero' trends of ensemble averages (illustrated in Figure 3) likely reflects the implication of averaging rather than a systematic bias of GHMs toward a low magnitude of change. As an implication, ensemble averages even though useful, should not be used as a sole ground to infer changes in floods, as it may undermine the actual magnitude of simulated trends. As a result, the following analyses will report the full range (and mean) of each trend characteristic estimated across all ensemble members to communicate the uncertainty underlying the results.

Table 3. Characteristics of trends in the MAX7 index over the 1971-2005 period across 3,666 locations for GSIM observed trends and GSWP3 simulated trends (six GHMs available). Trend mean and trend standard deviation are expressed in % change per decade. Correlation was obtained from GSIM observed trends and GSWP3 simulated trends for each GHM. Boldface texts represent values that reject the null-hypotheses outlined in Table 2 (hypothesis 1 to 4).

GHM	Trend mean	Trend stand. dev.	% of sig. inc. trends	% of sig. dec. trends	Corr. obs. trend
H08	**-1.9**	**8.3**	4.8	6.7	**0.42**
LPJmL	-2.2	**7.1**	4.5	7.3	**0.37**
PCR-GLOBWB	**0.1**	**7.7**	9.6	6.1	**0.46**
WaterGAP2	**-0.3**	**8.2**	8.5	4.2	**0.49**
MPI-HM	-2.1	**8.7**	5.6	7.5	**0.50**
ORCHIDEE	**-1.4**	**8.6**	7	8.2	**0.35**
GSIM (observation)	-2.4	9.9	7.5	12.1	-

Table 4 provides the results of the model-observation comparison using GCMHIND simulated trends (intra-model averages are shown while results of individual simulations are reported in section 4 of supplementary material). Similar to GSWP3 trends, intra-model averages (i.e. calculated from simulations of one GHM) of GCMHIND trends tend to have a higher global mean and lower trend standard deviation than observed. The composition between the percentages of locations showing significant trends varies substantially across simulations and statistical significance was found only for decreasing trends over three out of 21 simulations (two LPJmL simulations and one MPI-HM simulation). The multi-model ranges encapsulate the observed trend mean and percentage of significant trends, while the observed trend standard deviation is clearly above the range exhibited from all GCMHIND simulations. The significantly lower simulated trend standard deviation can be partially attributable to the coarse resolution of GHMs'

atmospheric/land surface inputs, which may not sufficiently reflect the variation of hydrological processes across small-to-medium size catchments.

Table 4. Characteristics of trends in the MAX7 index over the 1971-2005 period across 3,666 locations for GCMHIND simulated trends. Trend mean and trend standard deviation are expressed in % change per decade. Intra-model averages of trend characteristics are shown for each GHM. Values in the parentheses show the number of simulations rejecting the null hypothesis (from 1 to 4) outlined in Table 2 (out of four GCMs). Multi-model min/max/average values together with those exhibited from GSIM are also provided.

GHM	Trend mean	Trend stand. dev.	% of sig. inc. trends	% of sig. dec. trends	Corr. obs. trend
H08	-1.7 (4)	8.5 (4)	4.9 (0)	8.8 (0)	0.03 (2)
LPJmL	-2.3 (4)	7.9 (4)	4.2 (0)	12.6 (2)	0.09 (3)
PCR-GLOBWB	-1.1 (2)	7.4 (4)	7.5 (0)	9.4 (0)	0.06 (3)
WaterGAP2	-1.3 (4)	8.4 (4)	5.4 (0)	8.0 (0)	0.02 (2)
MPI-HM	-1.8 (3)	8.7 (3)	5.7 (0)	9.9 (1)	0.05 (2)
ORCHIDEE	-0.4 (2)	8.6 (2)	6.9 (0)	7.0 (0)	0.04 (1)
Multi-model min	-4.2	7.0	2.2	4.1	-0.06
Multi-model max	0.6	9.5	12.2	17.3	0.18
Multi-model average	-1.5	8.2	5.6	9.5	0.05
GSIM (observation)	-2.4	9.9	7.5	12.1	-

Among 21 GCMHIND simulations, the 'zero similarity' hypothesis (hypothesis 5) was rejected over 13 simulations, indicating that GCM-GHM ensemble members possess some capacity to simulate the spatial structure of observed trends in streamflow extremes. The correlation between GCMHIND simulated trends and GSIM observed trends, however, is significantly lower than that exhibited from GSWP3 simulated trends across all GHMs (reported at Table 3). The results of the similarity assessment are illustrated for a single GHM (H08; as the results were similar for other GHMs) in Figure 4, where the correlation between observed trends and GSWP3 simulated trends is significantly different from zero. In contrast, the correlation between observed trends and each of the simulated trends under hindcast atmospheric forcing (GCMHIND simulations) is much lower, with two of the four not being statistically higher than zero. These results confirm the substantial influence of atmospheric forcing on the simulated trend pattern relative to GHMs structure.

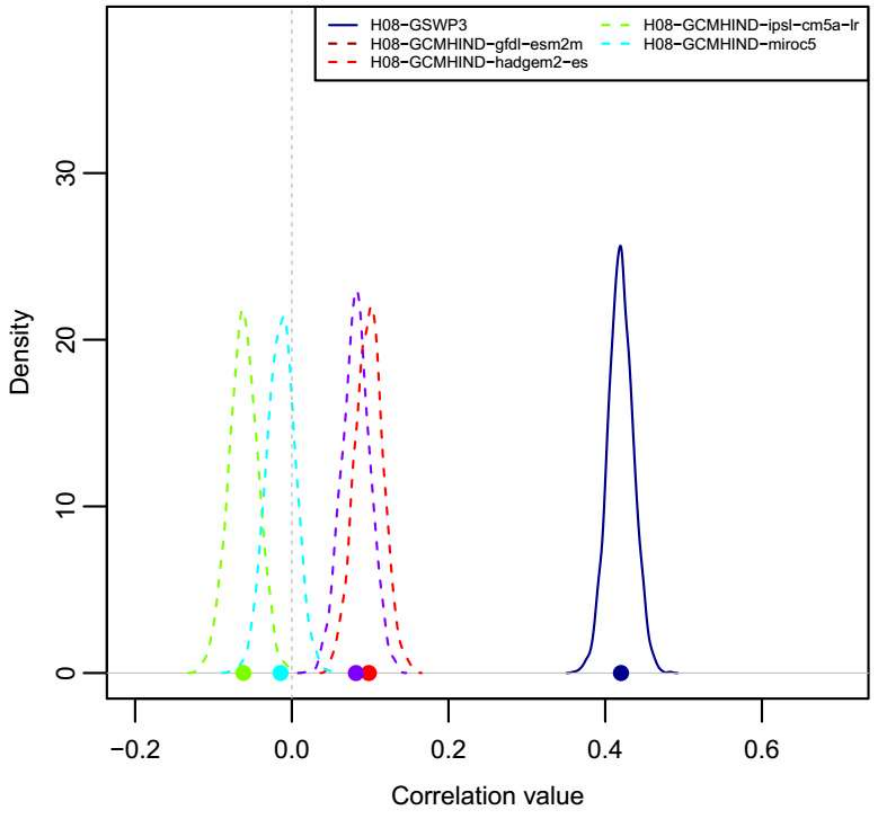

375

376 **Figure 4.** Model-observation correlation between observed trends and simulated trends across all simulations
377 (GSWP3 and four GCMHIND simulations) of a single model (H08; similar results for other GHMs). Coloured dots
378 indicate actual correlation between a specific simulated trend pattern and observed trend pattern across 3,666
379 locations. Colour lines represent the PDFs of correlation between simulated trend pattern and observed trend pattern
380 obtained through a bootstrap resampling procedure (B = 2000).

381

382 To further quantify changes at the regional scale, a model-observation comparison (identical to that at the global
383 scale) was conducted over six continents and the results are summarised in Table 5 (multi-model averages are
384 shown). The trend mean exhibited from GSIM ranges from -10.7% (Oceania) to 2.4% change per decade (Europe)
385 while trend standard deviation ranges from 8.3% (Europe) to 15.8% change per decade (Oceania). The percentage of
386 significant increasing (decreasing) trends exhibited from GSIM ranges from 3.2% to 22.6% (from 6.3% to 29.1%)
387 and the composition of significant trends across the six continents is consistent to a previous investigation (Do et al.,
388 2017). The observed percentage of significant trends is found to be above random chance for Europe (increasing
389 flood magnitude) and Australia (decreasing flood magnitude) and this feature is captured quite well by GSWP3
390 simulated trends, with at least half of the simulations confirming field significances detected from GSIM. Trend
391 characteristics simulated by GHMs at continental scale confirms some important findings from global scale

assessments, suggesting substantial uncertainty of trends in streamflow extremes introduced by GHMs at the continental scale:

- Both GSWP3 and GCMHIND simulations generally exhibit a higher trend mean and lower trend standard deviation compared to the observed trend at the continental scale (see also Section 3.1 of the supplementary).
- GCMHIND simulations generally exhibit lower capacity to reproduce trend characteristics relative to GSWP3 simulations due to the combined GHM-GCM uncertainty.

For GSWP3 simulations, the spatial correlation is weakest in Asia, as no simulation rejects the null-hypothesis of 'zero similarity', while the spatial correlation is strongest in Oceania (mainly southern Australia; correlation of 0.63). Oceania, however, exhibits the highest model-observation discrepancy in trend mean and trend standard deviation, indicating the capacity of a given GHM in terms of the trend spatial structure is not necessarily consistent with its performance in terms of the mean and spread of trends.

GCMHIND trends also suggest the opposite composition between percentages of significant trends compared to GSIM trends (e.g. simulated trends suggest more locations showing significant increasing trends while observed trends suggest the opposite). Among six continents, GCMHIND trends exhibited the lowest correlation (-0.14) in Oceania, whereas GSWP3 suggested the strongest correlation in this continent. This assessment further indicates the substantial impact of atmospheric forcing relative to GHM model structure on the simulated trends in high flow events. It is informative to note that this result is expected, as GCMs (although have been bias-corrected) generally have low capacity in reproducing the timing of wet/dry periods or the spatial distribution of climate extremes (Kiktev et al., 2007), and GHMs are likely to inherit these limitations when using GCMs' outputs as climate forcing data.

Table 5. Characteristics of trends exhibited from GSIM/GSWP3/GCMHIND streamflow dataset at the continental scale (each observation location of 3,666 sites was allocated into one of the six continents). For simulated trends, only the multi-model average is shown for each region. Trend mean and trend standard deviation are expressed in % change per decade. Values in the parentheses show the number of simulations rejecting the null-hypothesis described in Table 2 (up to six for GSWP3 simulations and 21 for GCMHIND simulations). For GSIM, field significance of increasing/decreasing trends was highlighted by boldface texts.

	No. of	**Trend mean**			**Trend Stand. Dev.**			**% sig. inc. trends**			**% sig. dec. trends**			**Corr. obs. trends**	
Region	**loc.**	*GSIM*	*GSWP3*	*GCMHIND*	*GSIM*	*GSWP3*	*GCMHIND*	*GSIM*	*GSWP3*	*GCMHIND*	*GSIM*	*GSWP3*	*GCMHIND*	*GSWP3*	*GCMHIND*
Asia	96	-3.1	-1.2 (4)	-2.7 (6)	8.8	6.6 (5)	7.2 (15)	4.2	4.2 (0)	2.2 (0)	15.6	10.3 (1)	9.7 (2)	0.07 (0)	0.11 (11)
N. America	2441	-3.5	-2.4 (3)	-1.6 (18)	9.4	7.9 (6)	8.0 (19)	3.2	2.8 (0)	5.3 (0)	13.4	7.5 (0)	9.3 (3)	0.38 (6)	0.03 (12)
Europe	730	2.4	2.6 (6)	-0.7 (17)	8.3	7.1 (5)	5.9 (21)	**22.6**	20.2 (3)	7.3 (1)	6.3	2.1 (0)	10.1 (4)	0.43 (6)	0.10 (13)
Africa	48	-2.5	-1.3 (0)	1.5 (12)	14.8	9.8 (5)	8.0 (20)	6.3	2.8 (0)	9.6 (2)	10.4	10.4 (0)	3.3 (0)	0.46 (6)	0.07 (6)
S. America	265	-2.0	-0.2 (5)	-3.6 (14)	10.1	7.6 (6)	10.0 (20)	7.9	7.2 (0)	3.4 (1)	10.2	4.4 (0)	13.4 (5)	0.26 (6)	0.18 (17)
Oceania	86	-10.7	-6.1 (4)	2.4 (21)	15.8	10.9 (6)	8.4 (21)	4.7	3.7 (0)	11 (2)	**29.1**	22.1 (4)	1.9 (0)	0.63 (6)	-0.14 (2)

3.2 Determining the representativeness of observation locations in the GHM simulations

To assess the representativeness of observations locations in GHM grid cells, trend characteristics obtained from all simulated grid cells were compared to those estimated from the observation locations (3,666 sites globally). For GSWP3 simulations, the results suggest a significant difference between trend characteristics from all model grid cells compared to those obtained from the observation locations (Table 6; multi-model averages shown). This feature is consistent at both global and continental scales, including North America and Europe – the continents with the best stream-gauge density. Specifically, the trend mean tends to get closer to zero, while the trend standard deviation obtained from all grid cells tends to be higher than that over observation locations. The difference between the percentages of significant increasing/decreasing trends across all grid cells also gets smaller. For instance, the percentage of observation locations showing significant increasing (decreasing) trends over Oceania is 3.7% (22.1%) for GSWP3 multi-model averages (reported in Table 5), while the corresponding values are 10.7% (15.1%) when all grid cells are considered (reported in Table 6). Additionally, field significance for increasing (decreasing) trends is detected in two (four) out of six simulations over Oceania, while the same feature could not be detected over the observation locations. These findings confirm that trends exhibited from observation locations are not a representative sample of trends obtained from all simulation grid cells, which has also been suggested through Figure 2. As a result, a common model-observation picture of changes in global flood hazard remains elusive. To enable a holistic perspective of changes in extreme flows, it is therefore crucial to improve not only models' capacity, but also data accessibility and expand streamflow observational networks to ensure unbiased samples are available for large scale investigations.

The findings using GCMHIND simulations are similar in terms of the trend mean (closer to zero) and trend standard deviation (higher) across all grid cells relative to the observation locations. Across all land areas, the composition of the percentages of land mass showing significant trends exhibited by GCMHIND simulations contradicts that obtained from the GSWP3 simulations for many continents. For example, GSWP3 simulations suggest more land areas showing significant decreasing trends than increasing trends over Asia and Oceania while GCMHIND simulations indicate an overall increasing change in extreme flows over the same continents. This feature further confirms the importance of uncertainty in atmospheric forcing in driving the spatial structure of the simulated trends, which will be explored further in the next section.

Table 6. Characteristics of simulated trends across all grid cells at both continental and global scales (multi-model averages are showed). For each simulation, cell-based trend mean/trend standard deviation was compared to that of gauge-based trends (reported in Table 4). Values in parentheses represent the number of simulations reject the null-hypothesis described in Table 2 (up to six simulations for GSWP3 and 21 simulations for GCMHIND). GSIM results are also provided for reference.

	Trend mean			**Trend Stand. Dev.**			**% sig. inc. trends**			**% sig. dec. trends**		
Region	*GSIM*	*GSWP3*	*GCMHIND*	*GSIM*	*GSWP3*	*GCMHIND*	*GSIM*	*GSWP3*	*GCMHIND*	*GSIM*	*GSWP3*	*GCMHIND*
Asia	-3.1	-0.7 (3)	0.4 (16)	8.8	10.3 (6)	9.0 (15)	4.2	7.7 (0)	9.6 (7)	15.6	9.9 (3)	7.7 (4)
N. America	-3.5	-1.8 (4)	0.4 (19)	9.4	10.3 (6)	8.3 (17)	3.2	6.9 (1)	8.2 (4)	13.4	12.3 (5)	6.6 (0)
Europe	2.4	1.1 (5)	0.2 (16)	8.3	8.5 (5)	8.4 (20)	**22.6**	11.5 (2)	9.1 (5)	6.3	4.5 (0)	7.9 (3)
Africa	-2.5	0.7 (2)	-1.7 (15)	14.8	11.0 (3)	10.1 (12)	6.3	10.9 (1)	8.5 (6)	10.4	11.2 (2)	15.5 (11)
S. America	-2.0	-2.0 (6)	-0.7 (19)	10.1	8.7 (3)	9.1 (17)	7.9	4.9 (0)	5.0 (0)	10.2	8.6 (0)	8.2 (1)
Oceania	-10.7	-1.0 (6)	0.5 (17)	15.8	11.3 (4)	10.4 (17)	4.7	10.7 (0)	10.3 (3)	**29.1**	15.1 (1)	9.6 (6)
Global	-2.4	-0.6 (6)	-0.1 (20)	9.9	10.3 (6)	9.4 (19)	7.5	8.3 (1)	8.6 (6)	12.1	10.2 (4)	9.0 (6)

3.3 The implication of simulation uncertainty on the projection of trends in flood hazard

This section focuses on the uncertainty in simulated trends under projected climate forcing at the global scale. For MPI-HM (no simulation for HadGEM2-ES forcing), streamflow was only simulated across the main stream-network (approximately 45% of the global land grid cells), and thus three simulations of this GHM were removed from the analysis. As a result, only 18 ensemble members were used to explore the uncertainty in projected trends (GCMRCP2.6 and GCMRCP6.0 – trends estimated for the 2006-2099 period and all cells were considered).

Table 7 shows a relatively low spread of the global trend mean (ranging from -1.3% to 0.8% change per decade; multi-model average of 0.0% change per decade for both GCMRCP2.6 and GCMRCP6.0) and trend standard deviation (ranging from 1.8% to 4.1% change per decade) across ensemble members. LPJmL and ORCHIDEE generally suggest a decreasing trend at the global scale, evident through the negative global mean and more grid cells showing significant decreasing trends. The standard deviation of trends in future simulations is substantially lower than the historical run (reported in Table 6). This feature is potentially due to the capacity of longer time series in capturing the inter-decadal variability of the streamflow regimes, with both dry and wet periods being considered (Hall et al., 2014). Projected trends under the RCP2.6 scenario generally have closer to zero mean and lower standard deviation compared to those introduced by the RCP6.0 scenario, reflecting the nature of an ambitious 'low-end warming' scenario, when anthropogenic climate change reaches its peak at the middle of the 21st century followed by a generally stable condition.

Interestingly, although most models suggest relatively moderate changes in the global trend mean, the composition between percentages of grid cells showing significant trends varies substantially, ranging from 7.5% (7.1%) to 30.1% (35.0%) for significant increasing (decreasing) trends at the 10% level, with RCP6.0 generally exhibits higher values. This finding indicates that inferences of changes focusing on global averages may mask significant regional trends, as there was a substantially high percentage of locations exhibiting significant increasing and decreasing trends exhibited in individual models.

Uncertainty in the spatial structure of trends in streamflow extremes is further investigated using both intra-model (to reflect GCM uncertainty) and inter-model correlations (to reflect the combined GCM-GHM uncertainty). A more robust spatial pattern of projected trends under RCP6.0 was found, indicated through generally higher intra-/inter-model correlation compared to those exhibited from trends simulated under RCP2.6 across all GHMs. This feature potentially reflects the less contrasted regional climate change of RCP2.6 relative to RCP6.0. The inter-model correlation is consistently lower than intra-model correlation due to the combined uncertainty of both GHMs and GCMs.

Table 7. The uncertainty in the characteristics of projected trends (GCMRCP2.6 and GCMRCP6.0) across 18 members at the global scale (five GHMs). Trend mean and trend standard deviation have unit of %-change per decade. At-site significance of trend was identified using Mann-Kendall test at 10% level and the percentage of grid cells showing significant increasing/decreasing trends was reported (no field significance test was conducted). Intra-model average value of each metric across is shown for each GHM (numbers of simulations are provided in the first column).

Model	No. of sim	Trend mean		Trend standard deviation		% of sig. inc. trends		% of sig. dec. trends		Intra-model correlation		Inter-model correlation	
		GCM RCP2.6	*GCM RCP6.0*	*GCM RCP2.6*	*GCM RCP6.0*	*GCM RCP2.6*	*GCM RCP6.0*	*GCM RCP2.6*	*GCM RCP6.0*	*GCM RCP2.6*	*GCM RCP6.0*	*GCM RCP2.6*	*GCM RCP6.0*
H08	4	0.1	0.3	2.5	3.4	14.2	22.1	11.6	19.3	0.17	0.41	0.02	0.21
LPJmL	4	-0.1	-0.2	2.1	3.0	10.0	19.1	9.4	19.7	0.04	0.41	0.01	0.18
ORCHIDEE	2	-0.5	-0.8	2.6	3.6	9.1	14.4	17.6	28.1	0.07	0.34	0.03	0.11
PCR-GLOBWB	4	0.1	0.0	2.4	3.4	15.1	22.7	11.6	20.2	0.07	0.30	0.02	0.18
WaterGAP2	4	0.2	0.5	2.3	3.0	13.0	25.9	8.0	11.8	0.03	0.25	0.01	0.17
Multi-model min	-	-0.6	-1.3	1.8	2.6	7.5	12.3	7.1	9.6	-0.03	0.12	-0.11	-0.18
Multi-model max	-	0.4	0.8	2.9	4.1	18.0	30.1	21.2	35.0	0.30	0.48	0.21	0.21
Multi-model average	-	0.0	0.0	2.3	3.2	12.6	21.6	11.0	18.9	0.08	0.34	0.01	0.04

To quantity the robustness in terms of regions with significant trends in streamflow extremes, the number of simulations showing significant increasing/decreasing trends was counted for each grid cell (value ranging from 0 to 18). As shown in Figure 5, the projections under RCP2.6 (top panels) do not suggest many regions with an increasing trend for most ensemble members, but consistently suggest decreasing trends over the majority of Africa, Australia and the western America. Although both scenarios suggested a similar spatial pattern, projections under the RCP6.0 scenario (lower panels) show a substantially higher robustness in terms of regions with significant changes over time in streamflow extremes. For instance, significant increasing trends are projected consistently over southern and south-eastern Asia, eastern Africa, and Siberia, while high agreement of decreasing trends is found over southern Australia, north-eastern Europe, the Mediterranean and north-western North America. These findings share some similarity with a previous investigation that used the ISIMIP Fast Track simulations (published before the ISIMIP2a and 2b simulations used here) to identify regions projected with an increasing magnitude of 30-year return level of river flow (Dankers et al., 2014). Specifically, both studies suggest overall: (1) an increasing trend over Siberia and South-East Asia; and (2) a decreasing trend over north-eastern Europe and north-western North America. The present study, however, additionally highlights a dominant decreasing trend over Australia, which was not shown previously. The different numbers of ensemble members (45 in Dankers et al. (2014) and 18 in the present study) and greenhouse gas concentration scenario (RCP8.5 in Dankers et al. (2014) and RCP2.6/RCP6.0 in the present study) between two studies indicate that the choice of GCM-GHM ensemble and greenhouse gas concentration scenarios could lead to substantially different projections of changes in flood hazard at the regional scale.

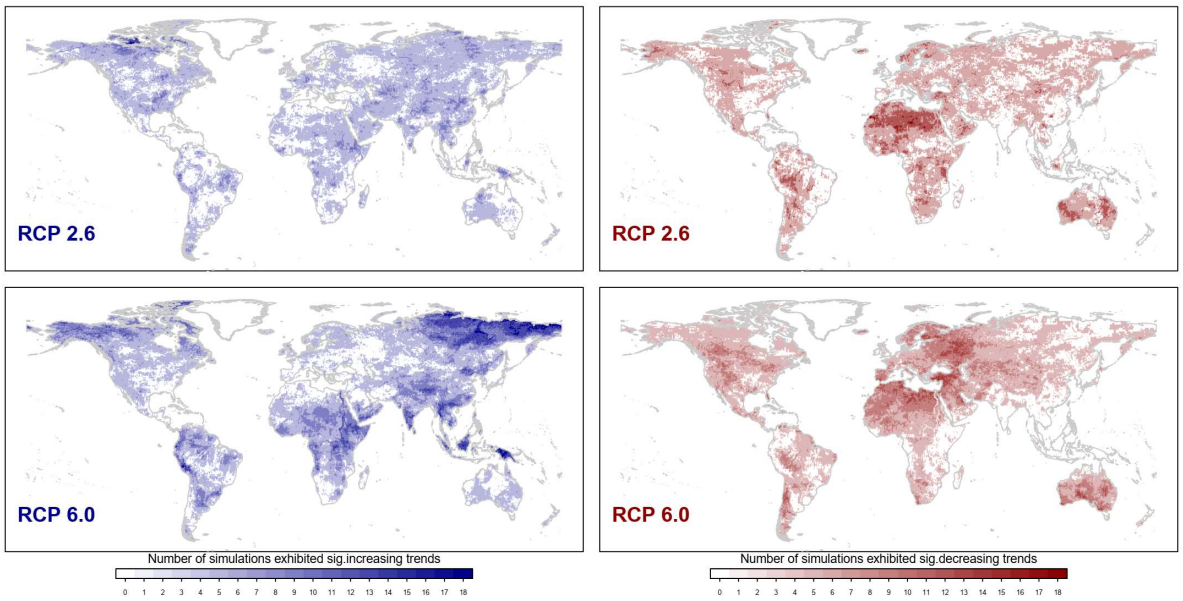

504

505 **Figure 5.** Number of simulations showing statistically significant trends at the 10% level at each grid cell. The left
506 panels show results for the assessment of increasing trends, while the right panels show results for significant
507 decreasing trends. Top: results of GCMRCP2.6 simulations; Bottom: results of GCMRCP6.0 simulations.

508

509 These results suggest the key role of GCM uncertainty in projections of changes in flood hazards, emphasising the
510 importance of a flexible adaptation strategy at the regional scale that can take this uncertainty into account (Dankers
511 et al., 2014) such as increasing flexibility in reservoir operations, and focusing on improved infrastructure resilience,
512 and safety to prepare for uncertain changes in the flood hazards. Such a strategy is achievable only through a reliable
513 and robust understanding of the change in flood hazard. The assessment of the representativeness of streamflow
514 observations (section 3.2), however, demonstrated that the observation locations selected for this assessment are not a
515 representative sample of the entire land mass. As a result, inference of changes in flood hazard may be biased toward
516 well-observed regions. To further highlight the potential impact of limitations in observed streamflow datasets, the
517 proportion of available stream gauges located in regions with different levels of projected 'flood risk' was assessed.
518 We first categorised each simulation grid-cell into one of the five 'flood-risk' groups. Note that in this analysis, "risk"
519 is defined as the number of simulations projecting a significant increasing trend, rather than the prominent definition
520 of risk as the combination of hazard, exposure and vulnerability (Kron, 2005). In this analysis, RCP6.0 scenario was
521 chosen as it yielded a higher global 'risk' of flood hazard relative to RCP2.6 scenario.

522 Figure 6 presents the percentage of all simulated grid cells (left panel) categorized in each of the five groups, and of
523 GSIM stations located in each group (right panel). As can be seen, 11.7% of grid cells fell into the "high risk" groups
524 (8.9% from Group 4 with 11-15 ensemble members, and 1.8% in Group 5 with 16-18 ensemble members), while

68.9% of grid cells fell into the “low risk” groups (22.0% for Group 1 with no ensemble members, and 46.9% for Group 2 with 1-5 ensemble members). Of all GSIM stations, only 0.9% are located in “high risk” grid cells (no station located in Group 5 grid cells) compared to 89.5% of stations located in “low risk” grid cells (35.4% for Group 1 and 54.1% for Group 2). The uneven distribution of stream gauges indicates potential difficulties in using observational records to provide an assessment of global or regional changes in flood hazard, which in part arises from data caveats associated with the spatiotemporal coverage and quality of observed gauge records across the globe. This finding further suggests the urgent demand for ongoing efforts to make streamflow observation more accessible. In addition. new innovations in remote sensing (Gouweleeuw et al., 2018), or development of runoff reanalysis (Ghiggi et al., 2019) should also be supported to complement the understanding of changes in floods for locations that were not observed by stream gauges.

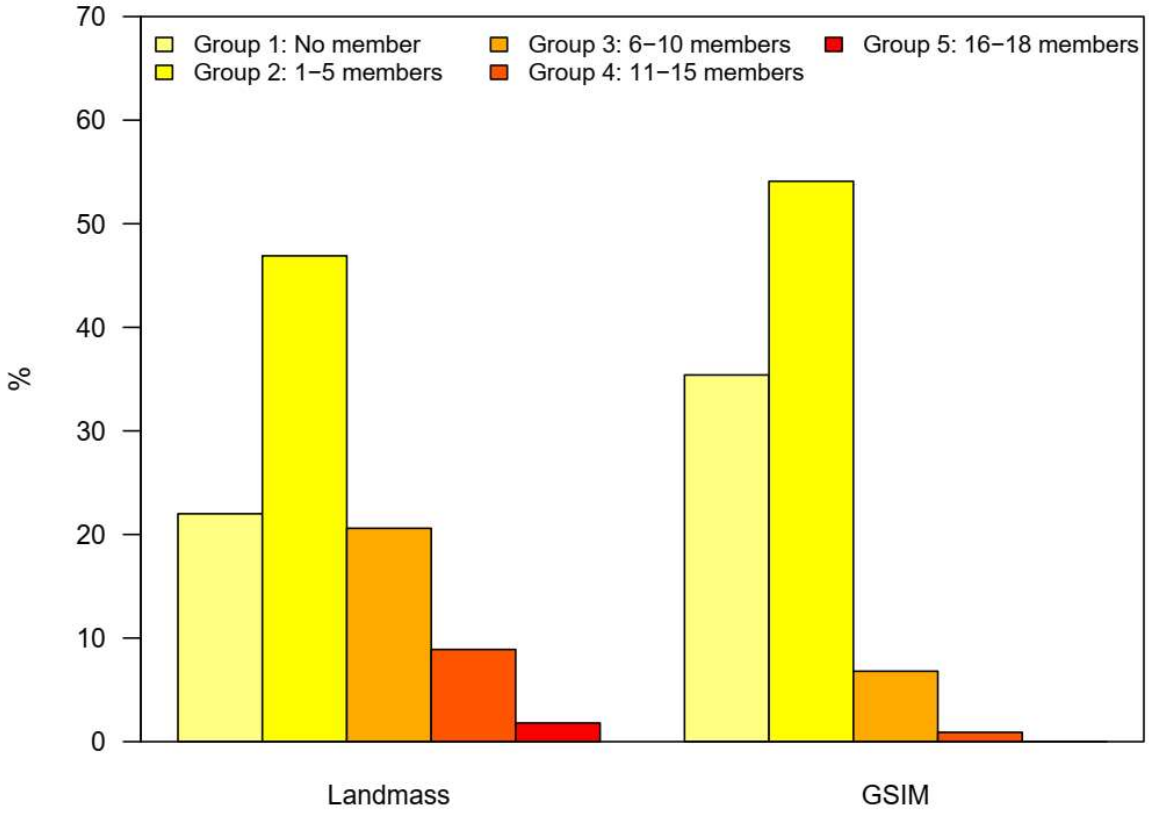

Figure 6. Percentage of grid-cell (“Landmass”) grouped by the number of simulations projecting a significant increasing trend under RCP6.0 scenario; and the percentage of streamflow stations (“GSIM”) assigned into each group. The range of possible simulations is from 0 to 18 and binned into five groups (Group 1: no members, Group 2: from 1 to 5 members, Group 3: from 6 to 10 members, Group 4: from 11 to 15 members and Group 5: from 16 to 18 members). To identify which group a specific station belongs to, the geographical coordinates of that station was superimposed on top of the global ‘flood-risk’ map.

4 Summary and conclusions

To explore the appropriateness of GHMs in simulating changes in flood hazards, this study evaluated the capacity of six GHMs to reproduce the characteristics of historical trends in 7-day annual maximum streamflow over the 1971-2005 period. The study also explored the implications of simulation uncertainty to projected changes in flood hazards over the 2006-2099 period. The findings of these investigations are summarized as follows.

1. Using observations from the Global Streamflow Indices and Metadata (GSIM) archive, this study confirms previous findings about changes in flood hazard over data-covered regions (Do et al., 2017), in which significant decreasing trends were found mostly in Australia, the Mediterranean region, western US, eastern Brazil and Asia (Japan and southern India), while significant increasing trends were more common over central US, southern Brazil, and the northern part of Western Europe.
2. Trends simulated by GHMs, when using an observational climate forcing, show moderate capacity to reproduce the characteristics of observed trends (i.e. the mean and standard deviation of trends, the percentage of stations showing significant increasing/decreasing trends, and the spatial structure of trends).
3. Climate variability and climate model uncertainty (i.e., the effect of using different GCMs to simulate the historical climate) significantly reduced the extent to which the GHMs' captured the observed spatial structure of trends. This was evident through significantly lower correlation between observed trends and simulated trends, when GCMs were used for the climate forcing, than when climate observations were used.
4. The simulated trends over observed areas inadequately represented spatially averaged trends simulated for wider spatial areas from all GHM grid cells at the continental and global scales. This was evident in most simulations for trend mean and trend standard deviation, indicating a potential bias toward well-observed regions of observation-based inferences about changes in flood hazard.
5. Under both RCP2.6 and RCP6.0 greenhouse gas concentration scenarios, simulated trends in 7-day maximum streamflow across ensemble members have relatively low uncertainty in terms of the global trend mean (ranging from -1.3% to 0.8% change per decade) and trend standard deviation (ranging from 1.8% to 4.1% change per decade).
6. Projected trends have wide spread of the percentage of land mass showing significant changes, ranging from 7.5% (7.1%) to 30.1% (35.0%) for significant increasing (decreasing) trends. This result indicates that limited changes to the global mean flood hazard could potentially mask out significant regional changes.
7. Projected trends in flood hazards show low inter-model spatial correlations (ranging from -0.18 to 0.21), indicating high uncertainty in future changes in flood hazards at the global scale. Under RCP6.0 scenario, some regions, e.g. south-eastern Asia, eastern Africa, Siberia, were consistently projected with significant

increasing trends, which has some similarity to previous findings that used ISIMIP Fast Track simulations (Dankers et al., 2014).

8. 'High-risk' regions (consistently projected with a significant increase in floods) of future changes in floods are sparsely sampled, covered by less than 1% of all available stream-gauges listed in the catalogue of GSIM. Data coverage, as a result, remains the key limitation of this study, which could potentially lead to an erroneous conclusion on the state-of-understanding of historical trends in flood hazard globally. Specifically, substantial changes, although having occurred, might not be captured by available streamflow records.

Our findings also show that individual models may provide contradictory signal of changes in flood hazards for a specific region, indicating high uncertainty in model-based inferences of changes in flood hazards. As a result, alternatives for the conventional approach in estimating changes in streamflow extremes at the global and regional scale (i.e. unweighted mean across all grid points) should be investigated. For instance, the spatial weighted averages (e.g. using inverse distance relative to observed locations as weights) could be used to compute global means of changes. Regional analysis using homogenised regions as the basis of reporting spatial domains (Zaherpour et al., 2018;Gudmundsson et al., 2019) could be a potential alternative for continental scale assessment.

The substantial discrepancy of trends simulated by different GHMs, despite having a common forcing boundary, represents another challenges in using GHM ensemble, as there are a wide range of factors that could contribute to these discrepancies. This study provides a (non-exhaustive) list of key differences across participated GHMs (supplementary Section 1) that could individually or collectively lead to different model outputs. Diagnosing the influence of these factors to models' capacity in simulating trends is still under-represented in the literature, and is an important research agenda for future investigations. For instance, the impact of different methods to simulate snow dynamic could be assessed by investigating model performances across catchments where snowmelt plays an (in)significant role in flood generations.

Improved performance of GHMs in terms of simulating changes in flood hazard, considering the many factors influencing model capacity, is achievable only through the combined efforts of many communities. The spread of trends in streamflow extremes (trend standard deviation) could be simulated more accurately by finer spatiotemporal resolution GHMs. Such an improvement in GHMs, however, is highly dependent on the quality of input datasets (e.g. dam operations, historical irrigation databases and land-use/land-cover, in addition to atmospheric forcing), which are driven by advances in other geophysical disciplines (Bierkens et al., 2015;Wood et al., 2011). The moderate capacity of GHMs in terms of simulating the spatial structure of trends in streamflow extremes indicates the need for improved representation of runoff generation at the global scale (e.g. to better reflect rainfall-runoff relationship and the

603 contribution of snow-dynamics), which is also a focus of large-sample hydrology (Gupta et al., 2014;Addor et al.,
604 2017). Uncertainty in GCMs, a long-standing challenge for the climate community, should also be addressed to
605 enable robust projections of flood hazard in a warmer climate. One possibility is through constraining model
606 performance using historical observations (to prevent climate models projecting an unrealistic state of the future
607 climate system such as atmosphere energy balance or cloud feedbacks), which could potentially reduce the
608 uncertainties of atmospheric forcing projections (Greve et al., 2018;Lorenz et al., 2018;He and Soden, 2016;Padrón et
609 al., 2019). In addition, future development of GHMs should also pay attention to model's capacity to simulate flood
610 timing, an important metric to represent flood generation processes (Blöschl et al., 2017;Hall and Blöschl, 2018;Do et
611 al., 2019). Integrating more sophisticated and effective routing schemes into future generations of GHM should also
612 be emphasized to ensure runoff is accurately converted into river discharge (Zhao et al., 2017).

613 This study presents a comprehensive investigation of historical and future changes in flood hazard using a hybrid
614 model-observation approach. The results highlighted a substantial difference between trend characteristics simulated
615 by GHMs and that obtained from GSIM archive. Our findings, therefore, suggest more attention should be paid to
616 investigating GHMs performance in the context of historical and future flood hazard, which is important for not only
617 the scientific community but also for stakeholders when using results of GHM simulations (Krysanova et al., 2018).
618 This is particularly important to determine the appropriateness of GHMs in specific investigations, as model
619 performance may vary substantially across different variables (e.g. moderate capacity in simulating spatial structure
620 of trends may be accompanied by a low performance in terms of simulating trend mean).

621 Large-sample evaluations, however, are highly dependent on data availability, which is one of the key barriers to a
622 holistic perspective of changes in floods. In this study, the unevenly distributed GSIM stations, partially due to the
623 constraint in data accessibility, do not provide representative samples at both global and continental scale. Sustained
624 and collective efforts from the broad hydrology community (Addor et al., 2019), therefore, are required to make
625 streamflow data becomes more FAIR (Findable, Accessible, Interoperable and Reusable; see Wilkinson et al., 2016),
626 and ultimately complement our limited understanding of flood hazards. Data providers, considering their tremendous
627 investments in maintaining and making streamflow observations publicly available, remain key agencies to enhance
628 the evidence-base of the global terrestrial water cycle and changes in flood hazard. The important contribution of
629 these agencies should be acknowledged appropriately when streamflow data being used. Centralised organisations
630 such as GRDC or WMO should also push forward the movement of making streamflow data accessible to the
631 research community. More initiatives based on citizen science (Paul et al., 2018) should be adopted, as this is a
632 potential option to crowdsource water data and offset the limitation of traditional observation system. Finally,

attention should also be paid to stream gauges maintenance, data housekeeping and data sharing to ensure ongoing flood monitoring is available to the present and future generations.

Acknowledgement

We thank two anonymous reviewers for their constructive comments that helped to improve the manuscript. Comments from Grabriele Villarini and Murray Peel to improve the manuscript are also appreciated. Hong Xuan Do is currently funded by School for Environment and Sustainability, University of Michigan through grant number U064474. This work was supported with supercomputing resources provided by the Phoenix HPC service at the University of Adelaide and Flux HPC service at the University of Michigan. The daily streamflow data sets were made publicly available from many data provider, including: the Global Runoff Data Centre (GRDC), the ARCTICNET initiative; the China Hydrology Data Project; The GEWEX Asian Monsoon Experiment – Tropics project; USGS National Data Services; Environment Canada; Brazilian National Water Agency; Spanish Center for Hydrographic Studies; Japanese Ministry of Land, Infrastructure, Transport and Tourism; Australian Bureau of Meteorology; Indian Central Water Commission.

References

Addor, N., Newman, A. J., Mizukami, N., and Clark, M. P.: The CAMELS data set: catchment attributes and meteorology for large-sample studies, Hydrol. Earth Syst. Sci. Discuss., 2017, 1-31, 10.5194/hess-2017-169, 2017.

Addor, N., Do, H. X., Alvarez-Garreto, C., Coxon, G., Fowler, K., and Mendoza, P.: Large-sample hydrology: recent progress, guidelines for new datasets and grand challenges, Hydrological Sciences Journal, 2019.

Alfieri, L., Burek, P., Feyen, L., and Forzieri, G.: Global warming increases the frequency of river floods in Europe, Hydrol. Earth Syst. Sci., 19, 2247-2260, 10.5194/hess-19-2247-2015, 2015.

Alfieri, L., Bisselink, B., Dottori, F., Naumann, G., de Roo, A., Salamon, P., Wyser, K., and Feyen, L.: Global projections of river flood risk in a warmer world, Earth's Future, n/a-n/a, 10.1002/2016EF000485, 2017.

Arnell, N. W., and Gosling, S. N.: The impacts of climate change on river flood risk at the global scale, Climatic Change, 1-15, 10.1007/s10584-014-1084-5, 2014.

Asadieh, B., and Krakauer, N. Y.: Global change in streamflow extremes under climate change over the 21st century, Hydrol. Earth Syst. Sci., 21, 5863-5874, 10.5194/hess-21-5863-2017, 2017.

Beck, H. E., van Dijk, A. I. J. M., de Roo, A., Dutra, E., Fink, G., Orth, R., and Schellekens, J.: Global evaluation of runoff from 10 state-of-the-art hydrological models, Hydrol. Earth Syst. Sci., 21, 2881-2903, 10.5194/hess-21-2881-2017, 2017.

Bennett, B., Leonard, M., Deng, Y., and Westra, S.: An empirical investigation into the effect of antecedent precipitation on flood volume, Journal of Hydrology, https://doi.org/10.1016/j.jhydrol.2018.10.025, 2018.

Berghuijs, W. R., Woods, R. A., Hutton, C. J., and Sivapalan, M.: Dominant flood generating mechanisms across the United States, Geophysical Research Letters, 43, 4382-4390, 10.1002/2016GL068070, 2016.

Biemans, H., Haddeland, I., Kabat, P., Ludwig, F., Hutjes, R. W. A., Heinke, J., von Bloh, W., and Gerten, D.: Impact of reservoirs on river discharge and irrigation water supply during the 20th century, Water Resources Research, 47, doi:10.1029/2009WR008929, 2011.

Bierkens, M. F. P., Bell, V. A., Burek, P., Chaney, N., Condon, L. E., David, C. H., de Roo, A., Döll, P., Drost, N., Famiglietti, J. S., Flörke, M., Gochis, D. J., Houser, P., Hut, R., Keune, J., Kollet, S., Maxwell, R. M., Reager, J. T., Samaniego, L., Sudicky, E., Sutanudjaja, E. H., van de Giesen, N., Winsemius, H.,

and Wood, E. F.: Hyper-resolution global hydrological modelling: what is next?, Hydrological Processes, 29, 310-320, 10.1002/hyp.10391, 2015.
Blöschl, G., Hall, J., Parajka, J., Perdigão, R. A. P., Merz, B., Arheimer, B., Aronica, G. T., Bilibashi, A., Bonacci, O., Borga, M., Čanjevac, I., Castellarin, A., Chirico, G. B., Claps, P., Fiala, K., Frolova, N., Gorbachova, L., Gül, A., Hannaford, J., Harrigan, S., Kireeva, M., Kiss, A., Kjeldsen, T. R., Kohnová, S., Koskela, J. J., Ledvinka, O., Macdonald, N., Mavrova-Guirguinova, M., Mediero, L., Merz, R., Molnar, P., Montanari, A., Murphy, C., Osuch, M., Ovcharuk, V., Radevski, I., Rogger, M., Salinas, J. L., Sauquet, E., Šraj, M., Szolgay, J., Viglione, A., Volpi, E., Wilson, D., Zaimi, K., and Živković, N.: Changing climate shifts timing of European floods, Science, 357, 588, 2017.
Blöschl, G., Hall, J., Viglione, A., Perdigão, R. A., Parajka, J., Merz, B., Lun, D., Arheimer, B., Aronica, G. T., and Bilibashi, A.: Changing climate both increases and decreases European river floods, Nature, 573, 108-111, 2019.
Burn, D. H., and Whitfield, P. H.: Changes in floods and flood regimes in Canada, Canadian Water Resources Journal / Revue canadienne des ressources hydriques, 41, 139-150, 10.1080/07011784.2015.1026844, 2016.
Burn, D. H., and Whitfield, P. H.: Changes in flood events inferred from centennial length streamflow data records, Advances in Water Resources, 121, 333-349, https://doi.org/10.1016/j.advwatres.2018.08.017, 2018.
CRED: The human cost of natural disasters: A global perspective, Centre for Research on the Epidemiology of Disasters, Brussels, 2015.
Cunderlik, J. M., and Ouarda, T. B. M. J.: Trends in the timing and magnitude of floods in Canada, Journal of Hydrology, 375, 471-480, http://dx.doi.org/10.1016/j.jhydrol.2009.06.050, 2009.
Dankers, R., Arnell, N. W., Clark, D. B., Falloon, P. D., Fekete, B. M., Gosling, S. N., Heinke, J., Kim, H., Masaki, Y., and Satoh, Y.: First look at changes in flood hazard in the Inter-Sectoral Impact Model Intercomparison Project ensemble, Proceedings of the National Academy of Sciences, 111, 3257-3261, 2014.
Do, H. X., Westra, S., and Michael, L.: A global-scale investigation of trends in annual maximum streamflow, Journal of Hydrology, 10.1016/j.jhydrol.2017.06.015, 2017.
Do, H. X., Gudmundsson, L., Leonard, M., and Westra, S.: The Global Streamflow Indices and Metadata Archive - Part 1: Station catalog and Catchment boundary, in, PANGAEA, 2018a.
Do, H. X., Gudmundsson, L., Leonard, M., and Westra, S.: The Global Streamflow Indices and Metadata Archive (GSIM) – Part 1: The production of a daily streamflow archive and metadata, Earth Syst. Sci. Data, 10, 765-785, 10.5194/essd-10-765-2018, 2018b.
Do, H. X., Westra, S., Leonard, M., and Gudmundsson, L.: Global-Scale Prediction of Flood Timing Using Atmospheric Reanalysis, Water Resources Research, 10.1029/2019wr024945, 2019.
Donat, M. G., Alexander, L. V., Yang, H., Durre, I., Vose, R., Dunn, R. J. H., Willett, K. M., Aguilar, E., Brunet, M., Caesar, J., Hewitson, B., Jack, C., Klein Tank, A. M. G., Kruger, A. C., Marengo, J., Peterson, T. C., Renom, M., Oria Rojas, C., Rusticucci, M., Salinger, J., Elrayah, A. S., Sekele, S. S., Srivastava, A. K., Trewin, B., Villarroel, C., Vincent, L. A., Zhai, P., Zhang, X., and Kitching, S.: Updated analyses of temperature and precipitation extreme indices since the beginning of the twentieth century: The HadEX2 dataset, Journal of Geophysical Research: Atmospheres, 118, 2098-2118, 10.1002/jgrd.50150, 2013.
FitzHugh, T. W., and Vogel, R. M.: The impact of dams on flood flows in the United States, River Research and Applications, 27, 1192-1215, 2011.
Forzieri, G., Feyen, L., Russo, S., Vousdoukas, M., Alfieri, L., Outten, S., Migliavacca, M., Bianchi, A., Rojas, R., and Cid, A.: Multi-hazard assessment in Europe under climate change, Climatic Change, 137, 105-119, 10.1007/s10584-016-1661-x, 2016.
Frieler, K., Lange, S., Piontek, F., Reyer, C. P. O., Schewe, J., Warszawski, L., Zhao, F., Chini, L., Denvil, S., Emanuel, K., Geiger, T., Halladay, K., Hurtt, G., Mengel, M., Murakami, D., Ostberg, S., Popp, A., Riva, R., Stevanovic, M., Suzuki, T., Volkholz, J., Burke, E., Ciais, P., Ebi, K., Eddy, T. D., Elliott, J., Galbraith, E., Gosling, S. N., Hattermann, F., Hickler, T., Hinkel, J., Hof, C., Huber, V., Jägermeyr, J., Krysanova, V., Marcé, R., Müller Schmied, H., Mouratiadou, I., Pierson, D., Tittensor, D. P., Vautard, R., van Vliet, M., Biber, M. F., Betts, R. A., Bodirsky, B. L., Deryng, D., Frolking, S., Jones, C. D., Lotze, H. K., Lotze-Campen, H., Sahajpal, R., Thonicke, K., Tian, H., and Yamagata, Y.: Assessing the impacts of 1.5 °C global warming – simulation protocol of the Inter-Sectoral Impact Model Intercomparison Project (ISIMIP2b), Geosci. Model Dev., 10, 4321-4345, 10.5194/gmd-10-4321-2017, 2017.
Galton, F.: Regression towards mediocrity in hereditary stature, The Journal of the Anthropological Institute of Great Britain and Ireland, 15, 246-263, 1886.

Ghiggi, G., Humphrey, V., Seneviratne, S. I., and Gudmundsson, L.: GRUN: an observation-based global gridded runoff dataset from 1902 to 2014, Earth Syst. Sci. Data, 11, 1655-1674, 10.5194/essd-11-1655-2019, 2019.
Giuntoli, I., Villarini, G., Prudhomme, C., and Hannah, D. M. J. C. C.: Uncertainties in projected runoff over the conterminous United States, 150, 149-162, 10.1007/s10584-018-2280-5, 2018.
Gosling, S., Schmied, M. H., Betts, R., Chang, J., Ciais, P., Dankers, R., Döll, P., Eisner, S., Flörke, M., Gerten, D., Grillakis, M., Hanasaki, N., Hagemann, S., Huang, M., Huang, Z., Jerez, S., Kim, H., Koutroulis, A., Leng, G., Liu, X., Masaki, Y., Montavez, P., Morfopoulos, C., Oki, T., Papadimitriou, L., Pokhrel, Y., Portmann, F. T., Orth, R., Ostberg, S., Satoh, Y., Seneviratne, S., Sommer, P., Stacke, T., Tang, Q., Tsanis, I., Wada, Y., Zhou, T., Büchner, M., Schewe, J., and Zhao, F.: ISIMIP2a Simulation Data from Water (global) Sector (V. 1.1), in, GFZ Data Services, 2019.
Gouweleeuw, B. T., Kvas, A., Gruber, C., Gain, A. K., Mayer-Gürr, T., Flechtner, F., and Güntner, A.: Daily GRACE gravity field solutions track major flood events in the Ganges–Brahmaputra Delta, Hydrol. Earth Syst. Sci., 22, 2867-2880, 10.5194/hess-22-2867-2018, 2018.
Greve, P., Gudmundsson, L., and Seneviratne, S. I.: Regional scaling of annual mean precipitation and water availability with global temperature change, Earth Syst. Dynam., 9, 227-240, 10.5194/esd-9-227-2018, 2018.
Gudmundsson, L., Tallaksen, L. M., Stahl, K., Clark, D. B., Dumont, E., Hagemann, S., Bertrand, N., Gerten, D., Heinke, J., Hanasaki, N., Voss, F., and Koirala, S.: Comparing Large-Scale Hydrological Model Simulations to Observed Runoff Percentiles in Europe, Journal of Hydrometeorology, 13, 604-620, 10.1175/JHM-D-11-083.1, 2012a.
Gudmundsson, L., Wagener, T., Tallaksen, L. M., and Engeland, K.: Evaluation of nine large-scale hydrological models with respect to the seasonal runoff climatology in Europe, Water Resources Research, 48, n/a-n/a, 10.1029/2011WR010911, 2012b.
Gudmundsson, L., Do, H. X., Leonard, M., and Westra, S.: The Global Streamflow Indices and Metadata Archive (GSIM) – Part 2: Quality control, time-series indices and homogeneity assessment, Earth Syst. Sci. Data, 10, 787-804, 10.5194/essd-10-787-2018, 2018.
Gudmundsson, L., Leonard, M., Do, H. X., Westra, S., and Seneviratne, S. I.: Observed Trends in Global Indicators of Mean and Extreme Streamflow, Geophysical Research Letters, 46, doi:10.1029/2018GL079725, 2019.
Guerreiro, S. B., Fowler, H. J., Barbero, R., Westra, S., Lenderink, G., Blenkinsop, S., Lewis, E., and Li, X.-F.: Detection of continental-scale intensification of hourly rainfall extremes, Nature Climate Change, 8, 803-807, 10.1038/s41558-018-0245-3, 2018.
Guha-Sapir, D., Hoyois, P., and Below, R.: Annual Disaster Statistical Review 2014: The numbers and trends, UCL, 2015.
Guimberteau, M., Ducharne, A., Ciais, P., Boisier, J.-P., Peng, S., De Weirdt, M., and Verbeeck, H.: Testing conceptual and physically based soil hydrology schemes against observations for the Amazon Basin, Geoscientific Model Development, 7, 1115-1136, 2014.
Guimberteau, M., Zhu, D., Maignan, F., Huang, Y., Yue, C., Dantec-Nédélec, S., Ottlé, C., Jornet-Puig, A., Bastos, A., Laurent, P., Goll, D., Bowring, S., Chang, J., Guenet, B., Tifafi, M., Peng, S., Krinner, G., Ducharne, A., Wang, F., Wang, T., Wang, X., Wang, Y., Yin, Z., Lauerwald, R., Joetzjer, E., Qiu, C., Kim, H., and Ciais, P.: ORCHIDEE-MICT (v8.4.1), a land surface model for the high latitudes: model description and validation, Geosci. Model Dev., 11, 121-163, 10.5194/gmd-11-121-2018, 2018.
Gupta, H., Perrin, C., Bloschl, G., Montanari, A., Kumar, R., Clark, M., and Andréassian, V.: Large-sample hydrology: a need to balance depth with breadth, Hydrology and Earth System Sciences, 18, p. 463-p. 477, 2014.
Hall, J., Arheimer, B., Borga, M., Brázdil, R., Claps, P., Kiss, A., Kjeldsen, T. R., Kriaučiūnienė, J., Kundzewicz, Z. W., Lang, M., Llasat, M. C., Macdonald, N., McIntyre, N., Mediero, L., Merz, B., Merz, R., Molnar, P., Montanari, A., Neuhold, C., Parajka, J., Perdigão, R. A. P., Plavcová, L., Rogger, M., Salinas, J. L., Sauquet, E., Schär, C., Szolgay, J., Viglione, A., and Blöschl, G.: Understanding flood regime changes in Europe: a state-of-the-art assessment, Hydrol. Earth Syst. Sci., 18, 2735-2772, 10.5194/hess-18-2735-2014, 2014.
Hall, J., and Blöschl, G.: Spatial patterns and characteristics of flood seasonality in Europe, Hydrol. Earth Syst. Sci., 22, 3883-3901, 10.5194/hess-22-3883-2018, 2018.
Hanasaki, N., Kanae, S., Oki, T., Masuda, K., Motoya, K., Shirakawa, N., Shen, Y., and Tanaka, K.: An integrated model for the assessment of global water resources–Part 2: Applications and assessments, Hydrology and Earth System Sciences, 12, 1027-1037, 2008a.

790 Hanasaki, N., Kanae, S., Oki, T., Masuda, K., Motoya, K., Shirakawa, N., Shen, Y., and Tanaka, K.: An
791 integrated model for the assessment of global water resources–Part 1: Model description and input
792 meteorological forcing, Hydrology and Earth System Sciences, 12, 1007-1025, 2008b.
793 Hannah, D. M., Demuth, S., van Lanen, H. A. J., Looser, U., Prudhomme, C., Rees, G., Stahl, K., and
794 Tallaksen, L. M.: Large-scale river flow archives: importance, current status and future needs,
795 Hydrological Processes, 25, 1191-1200, 10.1002/hyp.7794, 2011.
796 He, J., and Soden, B. J.: The impact of SST biases on projections of anthropogenic climate change: A
797 greater role for atmosphere - only models?, Geophysical Research Letters, 43, 7745-7750, 2016.
798 Hodgkins, G. A., Whitfield, P. H., Burn, D. H., Hannaford, J., Renard, B., Stahl, K., Fleig, A. K., Madsen,
799 H., Mediero, L., Korhonen, J., Murphy, C., and Wilson, D.: Climate-driven variability in the occurrence of
800 major floods across North America and Europe, Journal of Hydrology, 552, 704-717,
801 http://dx.doi.org/10.1016/j.jhydrol.2017.07.027, 2017.
802 Hoegh-Guldberg, O., Jacob, D., Taylor, M., Bindi, M., Brown, S., Camilloni, I., Diedhiou, A., Djalante, R.,
803 Ebi, K., and Engelbrecht, F.: Impacts of 1.5 ºC global warming on natural and human systems, 2018.
804 Hunger, M., and Döll, P.: Value of river discharge data for global-scale hydrological modeling, Hydrology
805 and Earth System Sciences Discussions, 12, 841-861, 2008.
806 IPCC: Managing the Risks of Extreme Events and Disasters to Advance Climate Change Adaptation,
807 Cambridge University Press, Cambridge, UK, and New York, NY, USA, 2012.
808 Ishak, E., Rahman, A., Westra, S., Sharma, A., and Kuczera, G.: Evaluating the non-stationarity of
809 Australian annual maximum flood, Journal of Hydrology, 494, 134-145, 2013.
810 Ivancic, T., and Shaw, S.: Examining why trends in very heavy precipitation should not be mistaken for
811 trends in very high river discharge, Climatic Change, 1-13, 10.1007/s10584-015-1476-1, 2015.
812 Johnson, F., White, C. J., van Dijk, A., Ekstrom, M., Evans, J. P., Jakob, D., Kiem, A. S., Leonard, M.,
813 Rouillard, A., and Westra, S.: Natural hazards in Australia: floods, Climatic Change, 1-15,
814 10.1007/s10584-016-1689-y, 2016.
815 Kettner, A. J., Cohen, S., Overeem, I., Fekete, B. M., Brakenridge, G. R., and Syvitski, J. P.: Estimating
816 Change in Flooding for the 21st Century Under a Conservative RCP Forcing: A Global Hydrological
817 Modeling Assessment, Global Flood Hazard: Applications in Modeling, Mapping, and Forecasting, 157-
818 167, 2018.
819 Kiktev, D., Sexton, D. M., Alexander, L., and Folland, C. K.: Comparison of modeled and observed trends
820 in indices of daily climate extremes, Journal of Climate, 16, 3560-3571, 2003.
821 Kiktev, D., Caesar, J., Alexander, L. V., Shiogama, H., and Collier, M.: Comparison of observed and
822 multimodeled trends in annual extremes of temperature and precipitation, Geophysical research letters, 34,
823 2007.
824 Kim, H.: Global Soil Wetness Project Phase 3 Atmospheric Boundary Conditions (Experiment 1), in, Data
825 Integration and Analysis System (DIAS), 2017.
826 Kron, W.: Flood Risk = Hazard • Values • Vulnerability, Water International, 30, 58-68,
827 10.1080/02508060508691837, 2005.
828 Krysanova, V., Donnelly, C., Gelfan, A., Gerten, D., Arheimer, B., Hattermann, F., and Kundzewicz, Z.
829 W.: How the performance of hydrological models relates to credibility of projections under climate change,
830 Hydrological sciences journal, 63, 696-720, 2018.
831 Kumar, S., Merwade, V., Kinter III, J. L., and Niyogi, D.: Evaluation of temperature and precipitation
832 trends and long-term persistence in CMIP5 twentieth-century climate simulations, Journal of Climate, 26,
833 4168-4185, 2013.
834 Kundzewicz, Z. W., Graczyk, D., Maurer, T., Przymusińska, I., Radziejewski, M., Svensson, C., and
835 Szwed, M.: Detection of change in world-wide hydrological time series of maximum annual flow, Global
836 Runoff Date Centre, Koblenz, Germany, 2004.
837 Leonard, M., Metcalfe, A., and Lambert, M.: Frequency analysis of rainfall and streamflow extremes
838 accounting for seasonal and climatic partitions, Journal of hydrology, 348, 135-147, 2008.
839 Liu, X., Tang, Q., Cui, H., Mu, M., Gerten, D., Gosling, S. N., Masaki, Y., Satoh, Y., and Wada, Y.:
840 Multimodel uncertainty changes in simulated river flows induced by human impact parameterizations,
841 Environmental Research Letters, 12, 025009, 10.1088/1748-9326/aa5a3a, 2017.
842 Lorenz, R., Herger, N., Sedláček, J., Eyring, V., Fischer, E. M., and Knutti, R.: Prospects and caveats of
843 weighting climate models for summer maximum temperature projections over North America, Journal of
844 Geophysical Research: Atmospheres, 123, 4509-4526, 2018.
845 Mallakpour, I., and Villarini, G.: The changing nature of flooding across the central United States, Nature
846 Clim. Change, 5, 250-254, 10.1038/nclimate2516, 2015.

Mangini, W., Viglione, A., Hall, J., Hundecha, Y., Ceola, S., Montanari, A., Rogger, M., Salinas, J. L., Borzì, I., and Parajka, J.: Detection of trends in magnitude and frequency of flood peaks across Europe, Hydrological Sciences Journal, 63, 493-512, 10.1080/02626667.2018.1444766, 2018.
Miao, Q.: Are We Adapting to Floods? Evidence from Global Flooding Fatalities, Risk Analysis, 0, doi:10.1111/risa.13245, 2018.
Mueller Schmied, H., Adam, L., Eisner, S., Fink, G., Flörke, M., Kim, H., Oki, T., Portmann, F. T., Reinecke, R., and Riedel, C.: Variations of global and continental water balance components as impacted by climate forcing uncertainty and human water use, Hydrology and Earth System Sciences, 20, 2877-2898, 2016.
Müller Schmied, H., Eisner, S., Franz, D., Wattenbach, M., Portmann, F. T., Flörke, M., and Döll, P.: Sensitivity of simulated global-scale freshwater fluxes and storages to input data, hydrological model structure, human water use and calibration, Hydrology and Earth System Sciences, 18, 3511-3538, 2014.
Munich Re: NatCatSERVICE: Loss events worldwide 1980 – 2014 Munich Re, Munich, 10, 2015.
Padrón, R. S., Gudmundsson, L., and Seneviratne, S. I.: Observational Constraints Reduce Likelihood of Extreme Changes in Multidecadal Land Water Availability, Geophysical Research Letters, 46, doi:10.1029/2018GL080521, 2019.
Pall, P., Aina, T., Stone, D. A., Stott, P. A., Nozawa, T., Hilberts, A. G. J., Lohmann, D., and Allen, M. R.: Anthropogenic greenhouse gas contribution to flood risk in England and Wales in autumn 2000, Nature, 470, 382-385, http://www.nature.com/nature/journal/v470/n7334/abs/10.1038-nature09762-unlocked.html#supplementary-information, 2011.
Paul, J. D., Buytaert, W., Allen, S., Ballesteros-Cánovas, J. A., Bhusal, J., Cieslik, K., Clark, J., Dugar, S., Hannah, D. M., Stoffel, M., Dewulf, A., Dhital, M. R., Liu, W., Nayaval, J. L., Neupane, B., Schiller, A., Smith, P. J., and Supper, R.: Citizen science for hydrological risk reduction and resilience building, 5, e1262, 10.1002/wat2.1262, 2018.
Pokhrel, Y., Hanasaki, N., Koirala, S., Cho, J., Yeh, P. J.-F., Kim, H., Kanae, S., and Oki, T.: Incorporating Anthropogenic Water Regulation Modules into a Land Surface Model, Journal of Hydrometeorology, 13, 255-269, 10.1175/jhm-d-11-013.1, 2012.
Schaphoff, S., Heyder, U., Ostberg, S., Gerten, D., Heinke, J., and Lucht, W.: Contribution of permafrost soils to the global carbon budget, Environmental Research Letters, 8, 014026, 2013.
Sharma, A., Wasko, C., and Lettenmaier, D. P.: If Precipitation Extremes Are Increasing, Why Aren't Floods?, Water Resources Research, 0, doi:10.1029/2018WR023749, 2018.
Slater, L. J., Singer, M. B., and Kirchner, J. W.: Hydrologic versus geomorphic drivers of trends in flood hazard, Geophysical Research Letters, 42, 370-376, 10.1002/2014GL062482, 2015.
Smith, K.: Environmental hazards: assessing risk and reducing disaster, Routledge, 2003.
Stacke, T., and Hagemann, S.: Development and evaluation of a global dynamical wetlands extent scheme, Hydrology and Earth System Sciences, 16, 2915, 2012.
Stahl, K., Hisdal, H., Hannaford, J., Tallaksen, L., Van Lanen, H., Sauquet, E., Demuth, S., Fendekova, M., and Jordar, J.: Streamflow trends in Europe: evidence from a dataset of near-natural catchments, Hydrology and Earth System Sciences, 14, p. 2367-p. 2382, 2010.
Sutanudjaja, E. H., van Beek, R., Wanders, N., Wada, Y., Bosmans, J. H. C., Drost, N., van der Ent, R. J., de Graaf, I. E. M., Hoch, J. M., de Jong, K., Karssenberg, D., López López, P., Peßenteiner, S., Schmitz, O., Straatsma, M. W., Vannametee, E., Wisser, D., and Bierkens, M. F. P.: PCR-GLOBWB 2: a 5 arcmin global hydrological and water resources model, Geosci. Model Dev., 11, 2429-2453, 10.5194/gmd-11-2429-2018, 2018.
Swiss Re: Natural catastropes and man-made disaster in 2014, Swiss Reinsurance Company, Zurich, Switzerland, 52, 2015.
Veldkamp, T. I. E., Zhao, F., Ward, P. J., de Moel, H., Aerts, J. C., Schmied, H. M., Portmann, F. T., Masaki, Y., Pokhrel, Y., and Liu, X.: Human impact parameterizations in global hydrological models improve estimates of monthly discharges and hydrological extremes: a multi-model validation study, Environmental Research Letters, 13, 055008, 2018.
Wada, Y., Wisser, D., and Bierkens, M. F. P.: Global modeling of withdrawal, allocation and consumptive use of surface water and groundwater resources, Earth Syst. Dynam., 5, 15-40, 10.5194/esd-5-15-2014, 2014.
Warszawski, L., Frieler, K., Huber, V., Piontek, F., Serdeczny, O., and Schewe, J.: The inter-sectoral impact model intercomparison project (ISI–MIP): project framework, Proceedings of the National Academy of Sciences, 111, 3228-3232, 2014.
Wasko, C., and Sharma, A.: Global assessment of flood and storm extremes with increased temperatures, Scientific Reports, 7, 7945, 10.1038/s41598-017-08481-1, 2017.

Wasko, C., and Nathan, R.: Influence of changes in rainfall and soil moisture on trends in flooding, Journal of Hydrology, 575, 432-441, https://doi.org/10.1016/j.jhydrol.2019.05.054, 2019.
Westra, S., Alexander, L. A., and Zwiers, F. W.: Global Increasing Trends in Annual Maximum Daily Precipitation, Journal of Climate, 26, 15, 2013.
Westra, S., Fowler, H. J., Evans, J. P., Alexander, L. V., Berg, P., Johnson, F., Kendon, E. J., Lenderink, G., and Roberts, N. M.: Future changes to the intensity and frequency of short-duration extreme rainfall, Reviews of Geophysics, 52, 522-555, 10.1002/2014RG000464, 2014.
Wilkinson, M. D., Dumontier, M., Aalbersberg, I. J., Appleton, G., Axton, M., Baak, A., Blomberg, N., Boiten, J.-W., da Silva Santos, L. B., Bourne, P. E., Bouwman, J., Brookes, A. J., Clark, T., Crosas, M., Dillo, I., Dumon, O., Edmunds, S., Evelo, C. T., Finkers, R., Gonzalez-Beltran, A., Gray, A. J. G., Groth, P., Goble, C., Grethe, J. S., Heringa, J., 't Hoen, P. A. C., Hooft, R., Kuhn, T., Kok, R., Kok, J., Lusher, S. J., Martone, M. E., Mons, A., Packer, A. L., Persson, B., Rocca-Serra, P., Roos, M., van Schaik, R., Sansone, S.-A., Schultes, E., Sengstag, T., Slater, T., Strawn, G., Swertz, M. A., Thompson, M., van der Lei, J., van Mulligen, E., Velterop, J., Waagmeester, A., Wittenburg, P., Wolstencroft, K., Zhao, J., and Mons, B.: The FAIR Guiding Principles for scientific data management and stewardship, Scientific Data, 3, 160018, 10.1038/sdata.2016.18, 2016.
Willner, S. N., Levermann, A., Zhao, F., and Frieler, K.: Adaptation required to preserve future high-end river flood risk at present levels, 4, eaao1914, 10.1126/sciadv.aao1914 %J Science Advances, 2018.
Woldemeskel, F., and Sharma, A.: Should flood regimes change in a warming climate? The role of antecedent moisture conditions, Geophysical Research Letters, 43, 7556-7563, 10.1002/2016GL069448, 2016.
Wood, E. F., Roundy, J. K., Troy, T. J., van Beek, L. P. H., Bierkens, M. F. P., Blyth, E., de Roo, A., Döll, P., Ek, M., Famiglietti, J., Gochis, D., van de Giesen, N., Houser, P., Jaffé, P. R., Kollet, S., Lehner, B., Lettenmaier, D. P., Peters-Lidard, C., Sivapalan, M., Sheffield, J., Wade, A., and Whitehead, P.: Hyperresolution global land surface modeling: Meeting a grand challenge for monitoring Earth's terrestrial water, Water Resources Research, 47, n/a-n/a, 10.1029/2010WR010090, 2011.
Zaherpour, J., Gosling, S. N., Mount, N., Schmied, H. M., Veldkamp, T. I. E., Dankers, R., Eisner, S., Gerten, D., Gudmundsson, L., and Haddeland, I.: Worldwide evaluation of mean and extreme runoff from six global-scale hydrological models that account for human impacts, Environmental Research Letters, 2018.
Zaherpour, J., Mount, N., Gosling, S. N., Dankers, R., Eisner, S., Gerten, D., Liu, X., Masaki, Y., Müller Schmied, H., Tang, Q., and Wada, Y.: Exploring the value of machine learning for weighted multi-model combination of an ensemble of global hydrological models, Environmental Modelling & Software, 114, 112-128, https://doi.org/10.1016/j.envsoft.2019.01.003, 2019.
Zhan, C., Niu, C., Song, X., and Xu, C.: The impacts of climate variability and human activities on streamflow in Bai River basin, northern China, Hydrology Research, 44, 875-885, 10.2166/nh.2012.146, 2012.
Zhang, A., Zheng, C., Wang, S., and Yao, Y.: Analysis of streamflow variations in the Heihe River Basin, northwest China: Trends, abrupt changes, driving factors and ecological influences, Journal of Hydrology: Regional Studies, 3, 106-124, https://doi.org/10.1016/j.ejrh.2014.10.005, 2015.
Zhao, F., Veldkamp, T. I., Frieler, K., Schewe, J., Ostberg, S., Willner, S., Schauberger, B., Gosling, S. N., Schmied, H. M., and Portmann, F. T.: The critical role of the routing scheme in simulating peak river discharge in global hydrological models, Environmental Research Letters, 12, 075003, 2017.